The relative importance of wind and hydroclimate drivers in modulating ~~wind-blown~~ windblown dust emissions in Earth system models

Xinzhu Li[1], Longlei Li[2], Yan Feng[3], and Xin Xi[1]

[1]Department of Geological and Mining Engineering and Sciences, Michigan Technological University, Houghton, MI, USA
[2]Department of Earth and Atmospheric Sciences, Cornell University, Ithaca, NY, USA
[3]Environmental Science Division, Argonne National Laboratory, Lemont, IL, USA

Correspondence: Longlei Li (ll859@cornell.edu) and Xin Xi (xinxi@mtu.edu)

Abstract.

~~Dust emission is modulated~~ Windblown dust emissions are governed by near-surface wind speed and ~~land surface conditions . A better understanding of dust emission variability and relationship with its physical drivers is essential for explaining existing discrepancies~~ soil erodibility, the latter influenced by hydroclimate conditions and land use. Accurate representations of the influence of these drivers in Earth system models ~~(ESMs) and guiding future improvement. This study evaluates the consistency of 21 ESMs in representing the collective and relative influence of~~ is critical for reproducing historical dust variability and projecting dust responses to future climate and land-use changes. Here we evaluate the model consistency in simulating the interannual variability of dust emissions and quantify the variance explained by wind speed and ~~five hydroclimate variables in modulating the dust interannual variability across different climate zones . In hyperarid regions~~hydroclimate drivers within 21 Earth system models and three climate zones (hyperarid, arid and semiarid). In the hyperarid zone, the models ~~show~~ exhibit poor agreement in ~~simulating~~ dust variability, ~~but capture the dominant wind control, except for GFDL-ESM4 and CESM coupled with the Kok et al. (2014) scheme, which exhibit anomalously strong hydroclimate influence.~~ with only 10% out of 210 pairwise comparisons showing significant positive correlations. In arid and semiarid ~~regions, the dust variability is shaped by a dual~~ zones, the models display a dipole pattern driven by a "double-edged sword" effect of land surface memory: models with coherent hydroclimate variability ~~converge in dust responses, while~~ show improved agreement, whereas those with divergent hydroclimate representations ~~lead to~~ show increased disagreement. ~~Although all~~ Most models capture the ~~increasing importance of hydroclimate drivers with decreasing aridity, the magnitude and spatial pattern of this transition vary considerably, resulting in growing inconsistency in the relative importance of wind and hydroclimate drivers. Implementing~~ dominant influence of wind speed on dust emissions in hyperarid areas except GFDL-ESM4 and CESM2-CAM-Kok, which display large spatial variability and anomalously high sensitivity to soil moisture and precipitation, respectively. Incorporating the Kok et al. (2014) scheme in CESM and E3SM generally ~~enhances the hydroclimate influence compared to~~ amplifies the dust sensitivity to hydroclimate drivers and reduces the wind contribution to explained variance, e.g., from 56% to 46% for CESM and from 86% to 75% for E3SM in the arid zone. These findings underscore the ~~Zender et al. (2003) scheme. These findings reveal key structural differences in dust emission simulations in ESMs, and underscore the importance of improved~~

representations of hydroclimate variability need to improve the representations of near-surface winds in hyperarid areas and hydroclimate and land surface processes in predicting dust responses to climate variations and changesarid and semiarid areas to reduce model uncertainties in dust emission estimates.

1 Introduction

Wind-blown dust from dryland regions Windblown dust aerosol is an essential element of the Earth's biogeochemical cycle, but has become a global concern due to its transboundary, multifaceted wide-ranging impacts on the climate, public healthecosystems, agriculture, and socioeconomic well-beingsociety. Dust emission is modulated by a number of atmospheric and land surface parameters related to variables which can be grouped into three broad drivers: sediment supply, sediment availability, and wind erosivity, which collectively determine the dust event timing, location, duration, and intensityintensity, and impacts of dust events (Xi, 2023). The most abundant *sediment supply* is typically found in low relief areas with thick layers of fine, unconsolidated materials produced by generated via weathering, fluvial, and/or aeolian processes (Bryant, 2013). These fine sediments, however, are not always available for dust entrainment due to the protection of groundwater The *sediment availability* for airborne dust production is strongly affected by soil moisture and surface armoring , such as (e.g., vegetation, soil crusts, and crust, non-erodible particles (Bullard et al., 2011). The *sediment availability* is modulated primarily by hydroclimate variability and land use practices (e.g., desertification, afforestation) , coarse particles) which determine the minimum or *threshold wind velocity* required to initiate mobilization. dust mobilization (Bullard et al., 2011). To initiate dust emission, near-surface winds must be strong enough to exceed the threshold wind velocity. As a result, the *Wind wind erosivity* is dominated by rareinfrequent, high wind events which may last from minutes to days, depending on the meteorological mechanism (Knippertz, 2014)generate sufficient drag to mobilize soil particles via saltation and sandblasting mechanisms. Depending on the relative importance of the three drivers, dust emission may fall into one of three distinct regimes: *supply-limited*, where a lack of suitable-sized sediments restricts dust emission; *availability-limited*, where fine sediments are present but are protected against wind protected against erosion; and *transport capacity-limited*, where sediments are dry and exposed , but the but near-surface winds are too weak to initiate dust entrainmentmobilize the particles.

The physical three dust emission drivers have been incorporated into global coupled aerosol models or in global aerosol-climate models and Earth system models (ESMs) to represent the environmental control of capture the environmental controls on the dust cycle. In many models, sediment supply is represented by Dust emission schemes in many ESMs use a time-invariant dust source function which approximates the abundance of erodible materials on a scale of 0 to 1 (e.g., Ginoux et al., 2001; Zender et al., 2003) . High values are generally found in topographic depressions which contain thick layers of to represent the spatially varying sediment supply, with high values generally associated with topographic depressions containing abundant alluvial or lacustrine deposits (Prospero et al., 2002). Dust models generally assume (Ginoux et al., 2001; Prospero et al., 2002; Zender et al., 2003) . These areas are generally assumed to have an unlimited sediment supply, without accounting for sediment depletion or replenishment over time (Zhang et al., 2016a). The hydroclimate modulation of sediment availability is represented by multiple parameters or processes. A common approach involves scaling vertical dust fluxes by the strongly coupled with the hydroclimate

variability in ESMs. Specifically, a bare soil fraction ~~to account for the presence of~~ scaling factor is often used to exclude non-erodible surfaces ~~such as water, snow , and vegetation. Most models also incorporate the effect of soil moisture on the enhancement of threshold wind velocity (Fécan et al., 1999). In addition, a drag partition term is commonly used to reduce the wind~~ covered by snow or vegetation. Vegetation also increases surface roughness and reduces the wind stress acting on erodible surfaces~~in the presence of vegetation and surface roughness elements (Marticorena and Bergametti, 1995; Shao et al., 2011) . To account for the dependence on wind erosivity, horizontal dust fluxes are computed~~ , which can be represented by a drag partitioning scheme (Marticorena and Bergametti, 1995; Shao et al., 2011). In addition, ESMs incorporate the role of soil moisture in enhancing the threshold wind velocity or suppressing dust emissions if the soil water content exceeds a given threshold (e.g., Fécan et al., 1999). Finally, ESMs parameterize the horizontal dust flux as the third or fourth power of wind ~~speeds above the threshold velocity. Because of this nonlinear relationshipand~~ speed once the threshold wind velocity is reached. This nonlinear relationship, combined with the skewed distribution of wind speeds, ~~global dust emissions are dominated by rare, high wind events (Cowie et al., 2015; Bergametti et al., 2017). Accurate model representations of these wind events remains challenging~~ reflect the dominant contributions of rare, high-wind events to global dust emissions (Cowie et al., 2015; B . Representing dust-producing wind events in ESMs remains a major challenge, since peak-wind generation mechanisms ~~, such as downdrafts from moist convection,~~ (such as convective downdrafts) often occur at spatial scales smaller than the typical grid spacing of ~~global models (Cakmur et al., 2004; Grini et al., 2005; Zhang et al., 2016b)~~ESMs (Cakmur et al., 2004; Grini et al., 2005; Ridle .

The Aerosol Comparisons between Observations and Models (AeroCom) initiative and Coupled Model Intercomparison Project (CMIP) have facilitated the ~~comparison of~~ intercomparison of ESMs in simulating the global dust cycle ~~in ESMs (Textor et al., 2006; Huneeus et al., 2011; Kim et al., 2014; Wu et al., 2020; Gliß et al., 2021; Zhao et al., 2022; Kim et al., 2024) . In general, the contemporary dust~~ (Textor et al., 2006; Huneeus et al., 2011; Kim et al., 2014; Wu et al., 2020; Gliß et al., 2021; Zhao et a . Generally, the modern-day dust aerosol column burden is reasonably constrained by ground- and satellite-based aerosol optical depth (AOD) observations over continental outflow areas, resulting in better model agreement ~~than those in~~ compared to dust emission and deposition ~~. Knippertz and Todd (2012) argued~~ estimates. Knippertz and Todd (2012) suggested that model tunings to match satellite ~~observations—often through dust source functions—can~~ observations, e.g., via the use of dust source functions, induce a compensational effect between dust emission and deposition, both of which lack ~~reliable~~ observational constraints at global scales. ~~As a result, dust emissions exhibit substantial model discrepancies, as well as large biases in reproducing the observed dust variability (Huneeus et al., 2011; Wu et al., 2020; Gliß et al., 2021; Zhao et al., 2022). For example, Pu and Ginoux (2018) found that most CMIP5 models failed to capture the interannual variability of satellite-derived dust AOD, and misrepresented the relative influence of surface bareness and wind speed. Evan (2018) showed that CMIP5~~ Indeed, previous AeroCom and CMIP model intercomparisons consistently show large discrepancies in the global total and regional distribution of dust emissions (Huneeus et al., 2011; Wu et al., 2020; Gliß et al., 2021; Zhao et al., 2022). While most ESMs roughly capture the annual cycle of dust over major source regions, they struggle in reproducing the dust interannual variability and relationships with wind speed and soil bareness (Pu and Ginoux, 2018; Evan et al., 2014; Evan, 2018; Wu et al., 2018) . Recent studies suggested that all CMIP models failed to ~~reproduce African dust variability due to poor representations of~~

near-surface winds. Wu et al. (2018) reported that most CMIP5 models failed to reproduce the declining dust frequency in China during 1961–2005, due to misrepresentations of wind speed and precipitation variability capture the large increase of global dust burden since preindustrial times, likely due to inaccurate model representations of historical climate and land-use changes and/or the dust sensitivity to these changes Kok et al. (2023); Leung et al. (2025). Together, these studies underscore the persistent uncertainties and limited predictive capability of ESMs in simulating the response of windblown dust emissions to hydroclimate variability and land surface changes.

The model discrepancies and biases can can be explained, at least partly, be explained by different in part, by the choice of dust emission schemesand parameter tunings. Some dust schemes use predefined, time-invariant . Earlier-generation schemes relied on empirical, temporally-invariant dust source functions to represent the spatially varying soil erodibility, as well as simplified parameterizations of the saltation-sandblasting process. In contrast, physically based schemes use more mechanistic representations of the dust flux dependence on shift emissions towards satellite-observed hotspot regions (Ginoux et al., 2001; Zender et al., , whereas newer schemes adopt more mechanistic approaches that account for sediment availability as a function of land surface conditionsand sandblasting efficiency, thereby eliminating the need for dust source functions . While such schemes offer (Kok et al., 2014b). These process-based schemes also introduce more realistic parameterizations of sandblasting efficiency to represent the momentum transfer from salting soil grains to the entrainment of fine particles into the atmosphere (Zender et al., 2003; Kok et . With improved model physics, they require process-based schemes usually involve more extensive input parameters , some of which do not have reliable data sources or are not properly represented in the model (Marticorena and Bergametti, 1995; Shao et al., 1996; . One example is the with greater uncertainties. The choice of wind speed in dust flux calculations. Some models also varies: some schemes use 10-m winds wind speeds for simplicity, whereas while others use friction velocity, which more accurately represents better captures the wind stress exerted acting on soil surfaces . However, estimating friction velocity requires the specification of surface roughnesslength, a parameter that lacks robust global constraintsbut requires information on surface roughness. Because surface roughness length is poorly constrained by observations, models employ varying assumptions and tunings to account for its effects on dust emission (e.g., Peng et al., 2012; Albani et al., 2015; Tegen et al., 2019).

Even among ESMs coupled with the same dust scheme, substantial discrepancies can result from different model resolutions, ESMs can diverge substantially due to differences in model configurations (e.g., horizontal resolution, vertical levels), parameter tunings, and coupled physical parameterizations. For exampleinstance, the bare soil fraction is computed based on the land /water mask, land cover determined from land type, vegetation fraction, and snow coverareal extent, all of which may vary by modeldiffer between ESMs. In particular, vegetation fraction cover may be prescribed from a fixed climatology or computed interactivelywith dynamic vegetation simulations. Additional differences arise from the soil column representations simulated interactively. Further discrepancies may result from differences in soil properties (e.g., hydraulic conductivity), soil column structure (e.g., number of layers, layer thickness), soil thermal and hydraulic properties, and formulations of and thickness of layers), and hydrologic processes (e.g., precipitation, runoff, evaporation, and infiltration processes. Together, these processes affect the topsoil water content and ultimately), which ultimately determine the water content of top soil layers and consequently the threshold wind velocity. Furthermore, parameterizations of The soil moisture effect on threshold wind velocity is also treated inconsistently, e.g., in calculating the residue level below which soil moisture is assumed to have no

effects on dust emission (e.g., Fécan et al., 1999; Evans et al., 2016; Volodin and Kostrykin, 2016). Moreover, ESMs employ different parameterizations for planetary boundary layer ~~processes and subgrid-scale wind variability strongly affect the model capability in capturing the strong near-surface winds during dust emissions. Given~~ and subgrid processes, which affect the momentum transfer from the atmosphere to the surface. Because of the strong coupling between dust emission and ~~multiple atmospheric~~ boundary layer and land surface processes, it is not surprising that dust emission ~~fluxes~~ estimates are strongly model-dependent.

~~This study assesses the model consistency in representing the dust emission variability and~~ While past studies have documented the large model diversity in the ~~collective and~~ climatological dust cycle (e.g., Pu and Ginoux, 2018; Wu et al., 2020; Zhao et al., 2022; Arya , key questions remain as to whether current ESMs consistently capture the temporal variability of historical dust emissions and their sensitivities to wind and hydroclimate drivers. Addressing these questions is essential for understanding and reducing model uncertainties in projecting dust emission responses to future changes in climate and land use. In this study, we provide a detailed assessment of the interannual variability and physical drivers of dust emissions, by quantifying the inherent relative influence of ~~wind and hydroclimate drivers~~ near-surface wind speed and hydroclimate conditions in modulating the dust variability ~~. Analogous to Koster et al. (2009)'s interpretation of root-zone soil moisture, we treat~~ within a suite of state-of-the-art ESMs. Compared to previous studies, we shift the focus from climatological means to temporal variability and move beyond documenting uncertainties to diagnosing their physical origins, thereby offering critical insights for improving the dust representation in ESMs.

A major challenge in evaluating dust models is the lack of direct, global observational constraints on dust emission fluxes. While satellite-derived dust optical depth and long-term surface concentration records provide valuable insights into dust variability (e.g., Prospero and Lamb, 2003; Zender and Kwon, 2005; Ginoux et al., 2012), they integrate information from emission, transport, and deposition, making it difficult to isolate the emission process (the focus of this work). Therefore, rather than validating absolute model performance against observations, we focus on diagnosing the inter-model consistency of simulated dust emission variability. Here we treat model-simulated dust emission flux as ~~a~~ an unobservable, model-specific quantity, which is characterized by a dynamic range defined by the ~~dust scheme and coupled processes within individual ESMs. The~~ internal model variability, parameterizations, parameter uncertainties, and model configurations. This approach is analogous to Koster et al. (2009)'s view of root-zone soil moisture and reflects the fact that model-simulated dust emission fluxes ~~produced by various ESMs essentially represent different~~ cannot be validated with field observations. While model-simulated dust emissions are essentially approximations of the true state ~~which they are trying to reproducebut has no direct observations to validate against. As such, these fluxes are expected to differ in climatological means and variability characteristics. The true value of dust emission fluxes lies~~ they aim to reproduce, their true information content lie not necessarily in ~~their absolute magnitudes , but rather in their temporal variability and sensitivity to the~~ the absolute magnitudes but in their spatiotemporal variability and sensitivities to physical drivers. ~~If the variability of physical drivers is consistent between models, one would expect some degree of correlation in the simulated dust fluxes. For example, stronger winds combined with drier soils should lead to more emissions, regardless of which model is used. Given the large diversity of ESMs and dust emission parameterizations, the extent of inter-model agreement in the dust emission variability and sensitivity to physical~~

drivers remains poorly understood. In particular, the relative importance of wind erosivity and hydroclimate-driven sediment erodibility within individual ESMs has not been evaluated. By quantifying the collective and relative contributions of physical drivers in explaining the simulated dust variability in a family of ESMs and reanalysis products, relative influence of wind speed and hydroclimate conditions over different climate regimes (i.e., hyperarid, arid and semiarid), this study provides new insights into the model discrepancies and biases of global dust emission simulations. in dust emission representations.

The remainder of this paper is structured organized as follows. Section 2 describes the ESMs and aerosol reanalysis datasets reanalysis datasets considered in this study, and the dominance analysis technique used to quantify the joint and relative influence of dust emission drivers. Section 3 presents the intercomparison of climatological mean, spatial contribution and interannual variability of dust emissions, dust interannual variability and the relative importance of wind and hydroclimate driversinfluence of wind speed and hydroclimate conditions. The conclusions are summarized in Section 4.

2 Data and Approach

2.1 Global models ESMs and aerosol reanalysis products

Table 1 summarizes the dust emission parameterizations used in the ESMs and reanalysis products considered analyzed in this study. These include fully-coupled simulations from , which differ in model resolution, vegetation process, and dust emission parameterizations, among other aspects. Among the 21 ESMs, 18 are from the CMIP6 models for the period of 1950–2014. Unless otherwise specified, we historical, fully-coupled experiments (1980–2014). We use the first ensemble member (r1i1p1f1) from each model. In the , unless otherwise stated. CMIP6 archive, two configurations of the consists of several model families that share common heritage but differ in physics options and configurations. For instance, two Community Earth System Model (CESM) share the same configurations employ the dust scheme of Zender et al. (2003) (hereafter referred to as the Zender scheme) , but use different atmospheric modulesschemes: Community Atmosphere Model (CAMCESM2-CAM-Zender) vs. Whole Atmosphere Community Climate Model (WACCM). The key difference between CAM and WACCM lies in their CESM2-WACCM-Zender), with major differences in the vertical extent and representation of upper atmospheric processes. The three Three GISS-E2 models use the same dust scheme described in Miller et al. (2006) , but differ by of Miller et al. (2006) but differ in model version (2.1 vs. 2.2) and aerosol microphysics schemes: One-Moment Aerosol (OMA; ensemble member r1i1p3f1) vs. Multiconfiguration Aerosol TRacker of mIXing state (MATRIX; ensemble member r1i1p5f1) (Miller et al., 2021)(Miller et al., 2021; Rind et al., 2020). UKESM1.0 is built upon the HadGEM3-GC3.1 general circulation model, which share use the same dust scheme of Woodward (2001) , but differ in parameter tuning tunings and dust source representation representations (Woodward et al., 2022). Similarly, MIROC-ES2L is developed based on the MIROC model, both using the general circulation model version 5.2 (MIROC5) (Hajima et al., 2020), while MIROC6 incorporates updated physics which improved the mean climate state and internal variability relative to MIROC5 (Tatebe et al., 2019). Both MIROC-ES2L and MIROC6 adopt the dust scheme from SPRINTARS (Spectral Radiation-Transport Model for Aerosol Species) the SPRINTARS aerosol module (Takemura et al., 2009).

Table 1. Summary of ~~dust emission parameterizations in~~ the Earth system models and aerosol reanalysis datasets considered in this study. Dust source function (DSF~~,~~) column indicates whether an empirical dust source function is used. ~~u_*, friction velocity~~Leaf area index (LAI) column indicates whether LAI is a prognostic variable. ~~u~~D_m, ~~10-m wind speed~~dust particle diameter upper limit. ~~ω, soil moisture. r_0, surface roughness. ERS, European Remotes Sensing satellite.~~

Model	~~D_{max}~~ Resolution	D_m	Wind	DSF
CESM2-CAM-Zender	0.9°×1.25°	10	u_*^3	~~Zender et al. (2003), Truncate~~
CESM2-WACCM-Zender	~~Same as CESM2-CAM-Zender~~ 0.9°×1.25°	10	u_*^3	Y
CESM2-CAM-Kok	0.9°×1.25°	10	u_*^3	~~No DSF~~ N
E3SM2-Zender	~~Same as CESM2-CAM-Zender except using the original DSF.~~ 1°×1°	10	u_*^3	Y
E3SM3-Kok	~~Same as CESM2-CAM-Kok~~ 1°×1°	10	u_*^3	Y
CanESM5-1	2.8°×2.8°	Bulk	u_*^3	~~Tegen et al. (2002)~~ Y
CNRM-ESM2.1	1.4°×1.4°	20	u_*^3	~~No DSF~~ N
EC-Earth3-AerChem	2°×3°	20	u_*^3	~~Tegen et al. (2002)~~ Y
GISS-E2.1-OMA	2°×2.5°	32	~~u^3~~ u_{10}^3	~~Ginoux et al. (2001)~~ Y
GISS-E2.1-MATRIX	~~Same as GISS-E2.1-OMA~~ 2°×2.5°	32	u_{10}^3	Y
GISS-E2.2-OMA	~~Same as GISS-E2.1-OMA~~ 2°×2.5°	32	u_{10}^3	Y
GFDL-ESM4	1°×1.25°	20	u_*^3	~~Ginoux et al. (2001)~~ Y
HadGEM3-GC31	0.6°×0.8°	63	u_*^3	~~Ginoux et al. (2001)~~ Y
UKESM1.0	1.25°×1.9°	63	u_*^3	~~No DSF~~ N
INM-CM5.0	1.5°×2°	Bulk	u_*^4	~~No DSF~~ N
IPSL-CM6A-LR	1.26°×2.5°	Bulk	~~u^3~~ u_{10}^3	~~Schulz et al. (2009)~~ Y
MRI-ESM2.0	1.9°×1.9°	20	u_*^3	~~No DSF~~ N
MIROC6	1.4°×1.4°	10	~~u^3~~ u_{10}^3	~~No DSF~~ N
MIROC-ES2L	~~Same as MIROC6~~ 2.8°×2.8°	10	u_{10}^3	N
MPI-ESM-1.2	1.9°×1.9°	Bulk	u_*^3	~~Tegen et al. (2002)~~ Y
NorESM2	~~Same as CESM2-CAM-Zender~~ 0.9°×1.25°	10	u_*^3	Y
MERRA2	0.5°×0.63°	20	~~u^3~~ u_{10}^3	~~Ginoux et al. (2001)~~ Y
JRAero	~~Same as MRI-ESM2.0~~ 1.1°×1.1°	20	u_*^3	N

In addition to the CMIP6 archive, we ~~include three fully coupled simulations to assess the influence of dust emission parameterizations. These include a CESM simulation for 2004–2013 using the physically based~~ consider an updated CESM (2004–2013) with the dust scheme of Kok et al. (2014b) (hereafter the Kok scheme; CESM2-CAM-Kok) (Li et al., 2022a), and ~~two simulations from~~ the Energy Exascale Earth System Model (E3SM~~) for~~ , 1980–2014~~: one~~) using the Zender ~~scheme~~ (E3SM2-Zender) ~~, and the other using the Kok scheme~~ and Kok (E3SM3-Kok) ~~(Feng et al., 2022). The Zender and Kok schemes differ fundamentally in their representation of dust sources: the Zender scheme employs an empirical dust source function to shift emissions toward preferential regions and improve agreement with satellite observations, whereas the~~ schemes (Feng et al., 2022; Xie et al., 2025). The key difference between the two schemes is that the Kok scheme adopts ~~more physically based parameterizations of soil erodibility , thereby eliminating~~ physically based soil erodibility parameterizations and eliminates the use of empirical dust source functions unlike the Zender scheme. These paired ~~CESM and~~ experiments allow us to evaluate how the choice of dust schemes (Zender vs. Kok) or models (CESM vs. E3SM~~simulations allow evaluating how dust emission and its relationship with physical drivers respond to newly implemented dust parameterizations. It is worth noting ~~) affect dust emission simulations. Nonetheless, we should point out that CESM2-CAM-Kok simulates dust as mineral components ~~, leading to different optical properties compared to CESM2-CAM-Zender that assumes spatially constant dust properties without accounting for mineralogy (Li et al., 2024). These differences may influence the meteorological fields and dust emissions via different radiative feedback~~with observationally constrained mineral optical properties (Li et al., 2024) , whereas CESM2-CAM-Zender does not account for particle mineralogy and simulates different dust optical properties that may affect dust radiative feedback on meteorology. Also, E3SM3 includes extensive updates over E3SM2 that may affect the near-surface meteorological and land surface conditions relevant to dust emissions (Xie et al., 2025).

We ~~also~~ further compare the ESMs with two aerosol reanalysis products: Modern-Era Retrospective Analysis for Research and Applications version 2 (MERRA2, ~~1980–2014~~1980–2014) (Gelaro et al., 2017), and Japanese Reanalysis for Aerosol (JRAero, ~~2011–2017~~2011–2017) (Yumimoto et al., 2017). ~~Unlike the free-running, fully-coupled CMIP6 simulations driven by historical forcings,~~ MERRA2 ~~and JRAero compute dust emissions based on assimilated meteorological and land surface variables. Both reanalyses are generated using global aerosol transport models constrained by data assimilation of bias-corrected satellite aerosol observations. MERRA2 utilizes the~~ is produced by the GEOS-5 data assimilation system with radiatively-coupled Goddard Chemistry ~~, Aerosol , Radiation ,~~ Aerosol Radiation and Transport (GOCART) module~~within GEOS-5 modeling system, in which dust emission~~ . Dust emission in GOCART is represented using the Ginoux et al. (2001) ~~parameterization. JRAero ,~~ scheme. JRAero is produced by the Japan Meteorological Agency ~~, is based on the~~ MASINGAR mk-2 global aerosol transport model~~and assimilates value-added MODIS AOD (Yumimoto et al., 2017). JRAero simulates dust emissions using the~~ , which simulates dust emission using the Shao et al. (1996) energy-based scheme~~of Shao et al. (1996)~~, same as ~~that used in the~~ MRI-ESM2.0 ~~aerosol model component (MASINGAR mk-2r4c) (Yukimoto et al., 2019).~~ (Yumimoto et al., 2017; Y . The meteorological and land surface conditions in MERRA2 and JRAero are constrained by observational data assimilation, and thus are expected to better capture historical climate and land cover changes than the ESMs. MERRA2 and JRAero also benefit from assimilation of bias-corrected total AOD, which provides some constraint on the dust column burden but does not directly constrain dust emissions.

We evaluate the climatological mean, spatial distribution, and interannual variability of dust emissions using monthly outputs from the We evaluate the consistency between ESMs and reanalysis products . We focus on nine geographic regions and three climate zones, as illustrated in Fig. **??**. The nine geographic regionsare North Africa (NAF), Southern Africa (SAF), Middle East (MDE), Central Asia (CAS), East Asia (EAS), South Asia (SAS), Australia (AUS), North America (NAM), and South America (SAM). The in representing the interannual variability of total dust emission fluxes. To facilitate comparison across common dust-emitting regions, we divide global dust source areas into three climate zonesare : hyperarid, arid, and semiarid, defined based on the aridity index (AI) , which is calculated defined as the ratio of climatological 1970–2000 climatological mean precipitation to potential evapotranspiration over 1970–2000. Specifically, the using the data from Zomer et al. (2022) . The hyperarid zone is defined by as AI≤0.05, arid zone by as 0.05<AI≤0.2, and semiarid zone by as 0.2<AI≤0.5. As shown in Fig. **??**, hyperarid regions cover most of Using these climatologically defined zones allows us to assess model discrepancies over common dust-emitting areas. Figure 1 shows that the hyperarid zone primarily covers North Africa, the Middle EastArabian Peninsula, Iranian Plateau, and Tarim Basin. Arid and semiarid zones include other major dust sources, such as cover other major sources, including the Sahel (North Africa), Turan Depression (Central Asia), Gobi Desert (East Asia), Thar Desert (South Asia), Kalahari Desert (Southern Africa), Chihuahua Desert (North America), Patagonia steppe (South America), and the Great Sandy and Simpson Deserts (Australia). The rationale of this climate zone-based analysis is that the relative importance of wind speed versus hydroclimate conditions is expected to depend strongly on climate regime. Specifically, hyperarid areas are expected to be dominated by permanently dry, barren surfaces with very low hydroclimate variability, and thus dust emission is primarily controlled by wind speed. Whereas, the arid and semiarid zones are expected to exhibit increased precipitation and hydroclimate variability resulting in stronger influence on the sediment availability.

2.2 Dominance Analysisanalysis technique

Past studies have commonly used linear regression coefficients to quantify the influence of physical drivers on dust emission dust sensitivities to its physical drivers (e.g., Pu and Ginoux, 2016; Aryal and Evans, 2021; Zhao et al., 2022). In a multiple linear regressionframework, the coefficient associated with a given predictor , a regression coefficient represents the mean change in the response variable per unit change in that a given predictor, holding all other predictors constant. This interpretation , however, assumes mutual independence among predictors—an predictors, an assumption that is often violated in dust studies, where dust emission drivers such as precipitation, soil moisture, and specific humidity are strongly correlated with each otherby strong correlations among hydroclimate variables. As a result, the linear regression coefficients may yield misleading inference of the predictor influencepredictor importance. Moreover, the regression coefficients, standardized or not, may not provide a consistent measure of predictor importance across models direct comparison of predictor influence due to the varying dynamic ranges in different modelsESMs.

In this study, we apply the dominance analysis technique to quantify the overall influence and relative importance relative influence of wind and hydroclimate drivers in modulating dust emissions. The monthly dust flux is used as the target variable, while the following near-surface variables are used as predictors: 10-m wind speed, total precipitation (including both liquid and solid phases), water content in the uppermost soil layer (or soil moisture), 2-m specific humidity, 2-m air temperature, and leaf

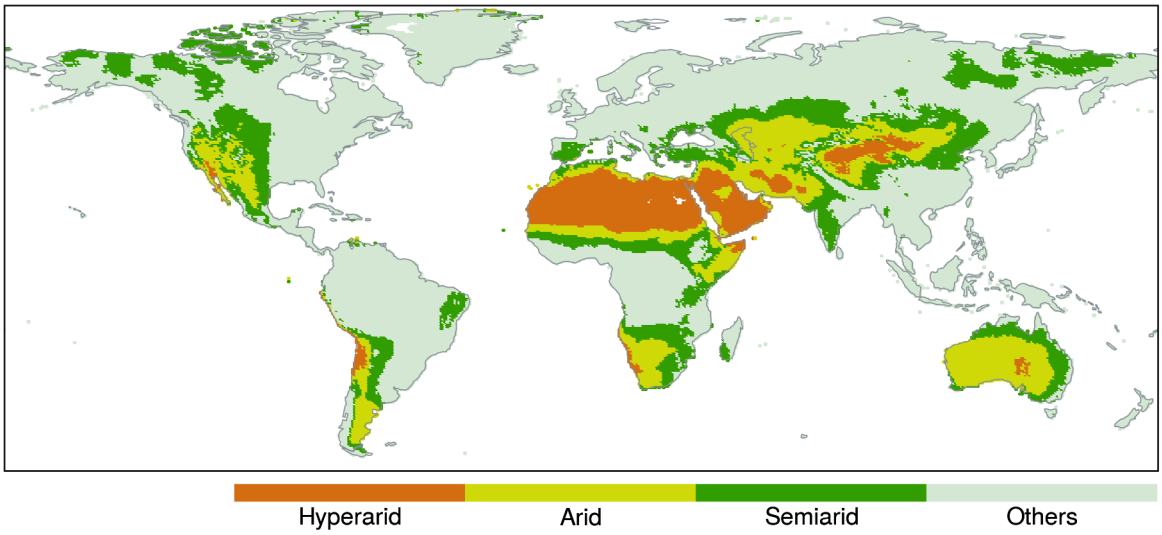

Figure 1. Definitions of ~~nine geographic regions~~ hyperarid, arid, and ~~three~~ semiarid climate zones~~analyzed in this study. The nine regions include: NAF (North Africa), SAF (Southern Africa), MDE (Middle East), CAS (Central Asia), EAS (East Asia), SAS (South Asia), AUS (Australia), NAM (North America), and SAM (South America).~~

~~area index (LAI). These predictors are either directly used as input parameters in dust flux calculations or serve as widely used proxies for dust emission drivers (e.g., Engelstaedter et al., 2003; Ravi et al., 2004; Zou and Zhai, 2004; Lee and Sohn, 2009; Cowie et al., . Among the predictors, wind speed represents the wind erosivity (hereafter referred to as the "wind" driver), while the remaining variables collectively characterize the hydroclimate influence on sediment erodibility (hereafter the "hydroclimate" driver).~~

~~Dominance analysis evaluates~~ on dust variability. Dominance analysis quantifies the marginal contribution of each predictor to the total explained variance (R^2) ~~by comparing~~ in the response variable by evaluating all possible subset models ($2^p - 1$ subsets for p predictors) in a multiple linear regression framework (Budescu, 1993; Azen and Budescu, 2003). ~~With six predictors, this yields 63 possible combinations of predictors.~~ For each predictor, the method calculates its average incremental contribution to the total R^2 across all subset models of the same size (i.e., models with the same number of predictors)~~. These values are then averaged across all subset sizes to yield~~ , and then average these values to obtain the predictor's unique contribution to the total R^2. A key ~~advantage of dominance analysis~~ property of this method is that the sum of ~~the individual~~ individual predictor contributions equals the R^2 of the full model (i.e., with all predictors included), thereby allowing the partitioning of ~~the total~~ explained variance among correlated predictors. The predictor-specific R^2 ~~among a common set of correlated predictorsin a consistent and comparable manner.~~ values can thus be interpreted as the portions of total variance in the response variable that are uniquely and jointly attributed to each predictor, accounting for their interactions and multicollinearity.

We use the monthly total dust emission flux as the response variable and consider six predictors: 10-m wind speed, total precipitation (including liquid and solid phases), water content in the uppermost soil layer (hereafter as soil moisture), 2-m specific humidity, 2-m air temperature, and leaf area index (LAI). The total dust emission flux is a bulk quantity that represents the source strength. Although ESMs differ in how they partition the total flux into discrete particle size bins—a key factor influencing dust transport and atmospheric lifetime—we expect the size partitioning to have minimal impact on diagnosing the emission process itself, particularly its sensitivity to the selected predictors. The primary drivers of emission variability operate upstream of the size partitioning of mobilized soil particles. The six predictors are chosen because they are either directly used as input parameters in dust flux calculations or strongly correlated with dust emission intensity, as suggested in numerous studies (e.g., Engelstaedter et al., 2003; RAVI et al., 2006; Zou and Zhai, 2004; Sokolik et al., 2021; Cowie et al., 2015; Kim and Choi, 20 . Among them, wind speed represents the wind erosivity driver, while the remaining variables collectively represent the hydroclimate effect on sediment availability.

Dominance analysis is performed for all ESMs and MERRA2 over grid cells with nonzero ~~dust emissions in ESMs and MERRA2 (~~emissions using deseasonalized and normalized data. JRAero is excluded from the dominance analysis due to missing predictors ~~). Grid-level results are then aggregated over predefined geographic regions and climate zones (Fig. ??) to assess the model consistency in the collective and relative influence of the selected predictors. Prior to the analysis, annual cycles are removed from both~~ and its short time span. We first subtract month-wise climatological means from the monthly dust fluxes and predictors, and ~~all variables are normalized to a 0–1 range using feature scaling to ensure equal weighting and comparability across predictors. In models where~~ then convert the deseasonalized data into 0–1 range via min-max normalization. For ESMs that use bare soil fraction ~~is used~~ as a scaling factor in dust flux calculations (e.g., ~~INM-CM5.0,~~ CNRM-ESM2.1, INM-CM5.0, UKESM1.0), the dust ~~fluxes are~~ flux is first normalized by the bare soil fraction in order to isolate the influence of the selected predictors. The grid-level total and predictor-specific R^2 values are used to assess the internal spatial variability (i.e., within each climate zone) and inter-model consistency in the total explained variance and predictor relative importance.

3 Results

3.1 Climatological ~~mean~~distribution

~~We begin by examining the climatological mean dust emission fluxes and comparing our results with previous assessments of AEROCOM and CMIP5 models.~~ Figure 2 displays the ~~mean~~ climatological mean annual dust fluxes from 21 ESMs, the model ensemble mean, and ~~the~~ MERRA2 and JRAero ~~reanalysis, averaged over 2005–2014 for all models except CESM2-CAM-Kok~~ datasets for the 2005–2014 period (2004–2013 ~~) and JRAero (~~for CESM2-CAM-Kok and 2011–2017 ~~). Most models~~ for JRAero). All datasets capture the global dust belt stretching from West Africa to East Asia, ~~along with~~ as well as the less intense sources in the Americas and Australia. E3SM3-Kok and HadGEM2-GC31 simulate the most ~~spatially~~ extensive dust-emitting areas ~~,~~ including high-latitude and subhumid ~~regions~~areas. In contrast, CESM2-CAM-Zender, CESM2-WACCM-Zender, and NorESM2 simulate discrete and limited dust-emitting areas ~~, due to the use of a truncated version of the Zender et al. (2003)~~ by excluding areas with dust source function ~~, which excludes grid cells with~~ values below 0.1. ~~Unlike CESM2-CAM-Zender,~~

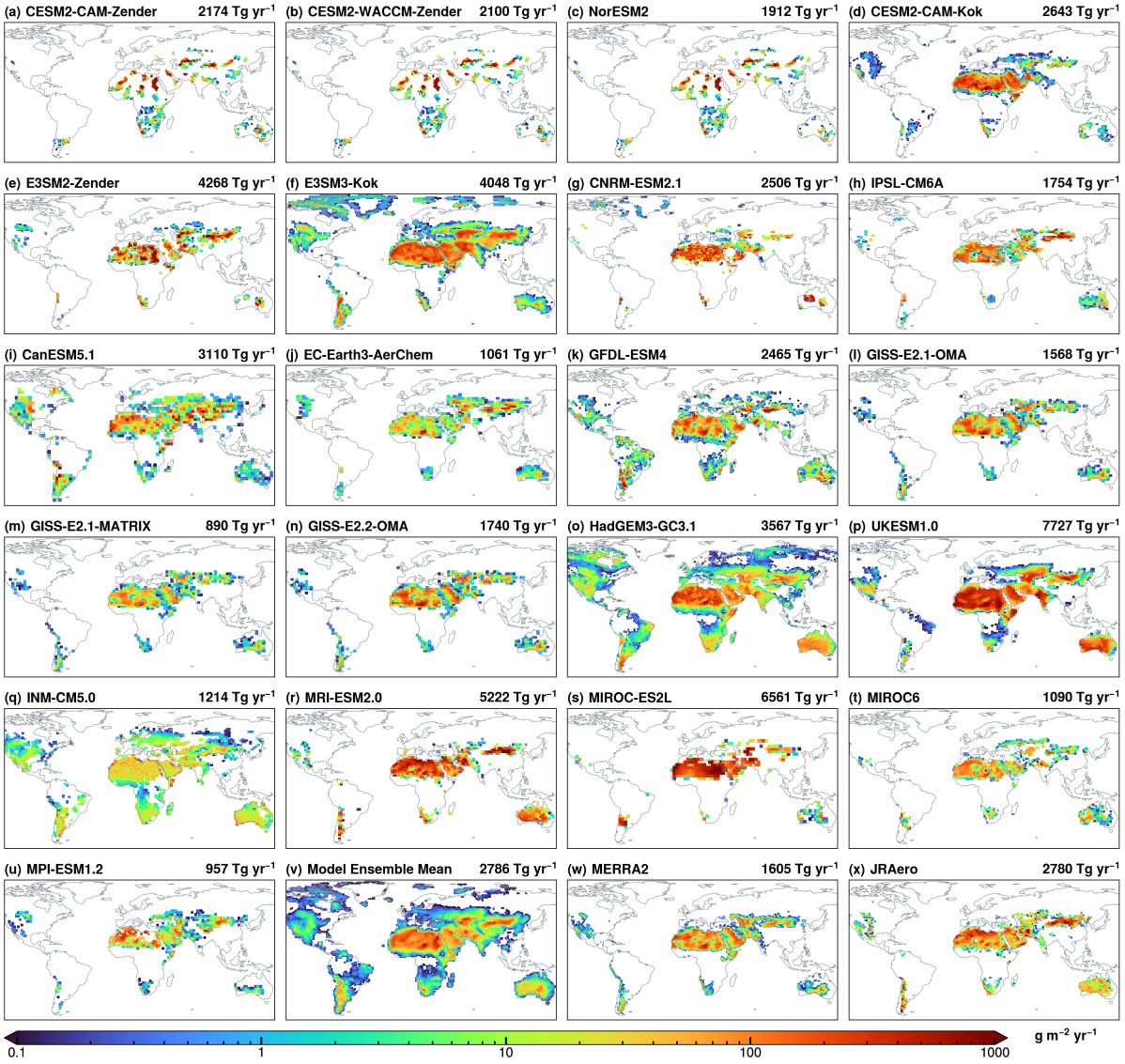

Figure 2. Climatological mean dust emission fluxes from (a–u) individual ~~ESMs~~Earth system models, (v) model ensemble mean, (w) MERRA2 reanalysis, and (x) JRAero reanalysis. Global annual total dust emissions are displayed on each panel.

E3SM2-Zender uses the original, ~~untruncated~~ unmodified Zender et al. (2003) dust source function and thus produces a more spatially continuous pattern (Fig. 2e).

~~Global annual total emissions vary~~ The global total dust flux varies greatly among the ESMs, ranging from 890 to 7727 Tg yr^{-1} ~~,~~ with nearly an order of magnitude difference (Fig. 2~~(a–u))~~a–2u). The model ensemble mean estimate is 2786 Tg yr^{-1} (Fig. 2v) ~~,~~ with a standard deviation of 1821 Tg yr^{-1}, corresponding to a diversity of 65% (defined as the ratio of standard deviation to ~~the~~ model ensemble mean). Based on ~~the 13 models which simulate particle diameters up to~~ models with a dust size upper limit of 20 μm, global ~~annual~~ dust emissions vary from 1062 to 6561 Tg yr^{-1} with a mean of 3012 Tg yr^{-1} and diversity of 51%. ~~The uncertainty ranges are~~ This uncertainty range is consistent with prior assessments. For example, Huneeus et al. (2011) compared 14 models from AeroCom Phase I and reported a global dust emission range of 500–4400 Tg yr^{-1} with a diversity of 58%. Out of the 14 models, 7 models considered ~~the diameter range of 0–20~~ particle diameters up to 20 μm and reported ~~an emission~~ a flux of 980–4300 Tg yr^{-1} with a diversity of 46%. Similarly, Gliß et al. (2021) compared 14 AeroCom Phase III models and found a range of 850–5650 Tg yr^{-1} with a diversity of 64%. Wu et al. (2020) reported a range of 740–8200 Tg yr^{-1} with a diversity of 66% ~~across~~ based on 15 CMIP5 models. Out of the 15 models, 7 models considering ~~the~~ a diameter range of 0–20 μm yielded 740–3600 Tg yr^{-1} with a diversity of 43%. More recently, Zhao et al. (2022) compared 15 models from the CMIP6 AMIP experiment and ~~found~~ reported a range of 1400–7600 Tg yr^{-1} with a diversity of 61%. ~~Collectively, these results along with our findings underscore persistent, substantial uncertainties in quantifying~~ Past studies, together with our results, indicate persistent large uncertainties in global dust emissions, despite improvements in model ~~physics, parameterizations, and spatial resolutions over time~~resolutions and physics.

The model ensemble mean global ~~annual dust emission rate~~ total dust flux is significantly higher than that of MERRA2 (1605 Tg yr^{-1}, Fig. 2w), but closely aligns with JRAero (2780 Tg yr^{-1}, Fig. 2x). ~~Overall~~In general, the model ensemble mean exhibits a more spatially ~~continuous and homogeneous pattern than MERRA2 and JRAero. Particularly, over the Sahara Desert, the model ensemble mean simulates relatively evenly distributed emissions,~~ homogeneous pattern over North Africa and Arabian Peninsula, whereas MERRA2 and JRAero display more ~~localized and clustered patterns, perhaps due to topographic constraints on sediment erodibility. Compared to MERRA2 and JRAero, the model ensemble mean shows lower emissions over the western and central Sahara, but higher emissions over the Libyan Desert and Nile River basin.~~ heterogeneous and localized patterns.

3.2 ~~Geographic distribution~~

~~Figure 3 a presents~~ Figure 3 displays the fractional contributions of ~~nine geographic regions~~ different climate zones to global dust emissions. ~~North Africa is identified across nearly all models as the largest source, contributing~~ The hyperarid zone accounts for more than half of ~~the global total . The model ensemble mean attributes approximately 54% of emissions to North Africa, compared to 59% in MERRA2 and 41% in JRAero.~~

~~Among the models,~~ global total emissions in most ESMs except two models: CanESM5.1 and INM-CM5.0, both of which simulate relatively uniform ~~emissions~~ emission patterns with less than 50% from the hyperarid zone (Fig. 2~~(i, q)), with only one-third of emissions originating from North Africa, substantially lower than other models. These deviations likely reflect~~

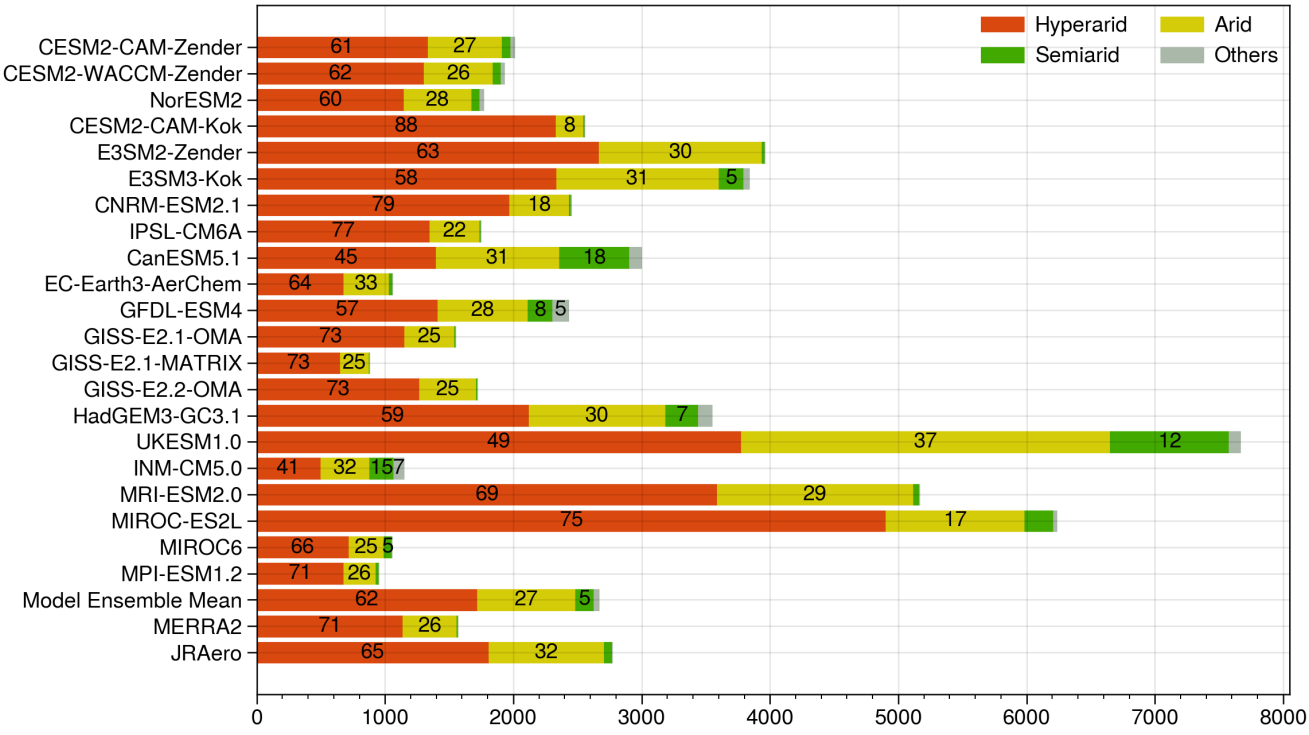

Figure 3. ~~Fractional contributions~~ Contributions of ~~dust emissions from~~ different ~~(a) geographic regions and (b)~~ climate zones to global annual dust emissions. Numbers indicate percentages above 5%.

~~known deficiencies and errors in CanESM5.1 and INM-CM5.0. In CanESM5.1~~i, 2q). This may be due to known deficiencies of these two models. As noted in Sigmond et al. (2023), improper parameter tuning related to the hybridization of dust tracers ~~has been shown to induce excessive mass corrections and~~ caused spurious dust events ~~, resulting in degraded representations of dust source distributions (Sigmond et al., 2023). In addition, an~~ and inaccurate dust distributions in CanESM5.1. An interpolation error in the bare soil fraction ~~distorted the~~ also distorted the model's dust source characterization, ~~leading to~~ resulting in poor agreement with satellite observations (Sigmond et al., 2023). In INM-CM5.0, ~~dust fluxes are calculated as the fourth power~~ the vertical dust flux is calculated as a function of friction velocity only, without accounting for the ~~effects of~~ dependence of threshold wind velocity on land surface conditions ~~on the erosion threshold (Volodin and Kostrykin, 2016). The over-simplified parameterization may produce biased dust emission simulations over regions where hydroclimate factors play an~~ (Volodin and Kostrykin, 2016; Volodin, 2022). While this simplification may be appropriate for the hyperarid zone, it can introduce significant biases over arid and semiarid zones where hydroclimate conditions play an increasingly important role in dust emissions.

Over the arid climate zone, the dust emission fraction ranges from 8% (CESM2-CAM-Kok) to 37% (UKESM-1.0), reflecting substantial discrepancies among the ESMs. These discrepancies become even larger over the semiarid zone, where the contribution

ranges from less than 1% to 18%. Three ESMs allocate more than 10% of dust to the semiarid zone: CanESM5.1 (18%), INM-CM5.0 (15%), and UKESM1.0 (12%). Thus, as the climate zone shifts from hyperarid to semiarid, the ESMs show larger discrepancies in their estimates of relative source strength. This climate zone-based comparison offers a first-order view of model representations of the dust sensitivity to hydroclimate conditions. Based on the model ensemble mean, global dust emissions are partitioned as 61% from hyperarid, 27% from arid, and 5% from semiarid zones. In contrast, MERRA2 and JRAero produce most dust from hyperarid and arid zones, with negligible contributions from the semiarid zone.

Among the ESMs, CESM2-CAM-Zender, CESM2-WACCM-Zender ~~,~~ and NorESM2 produce similar total emissions and regional fractions~~. The choice of CAM vs. WACCM causes minimal differences. Whereas, the choice of Zender vs. Kok dust scheme causes significant changes . Specifically, CESM2-CAM-Kok simulates 88% emissions from North Africa and the Middle East, significantly higher than~~ , suggesting that the choice between CAM and WACCM has minimal influence when the same dust scheme (Zender) is used. The paired CESM and E3SM experiments show different changes in regional fractions. For instance, the hyperarid zone fraction increases from 61% in CESM2-CAM-Zender ~~(56%). However,~~ to 88% in CESM2-CAM-Kok~~produces much less dust from East Asia (1% vs. 13% by CESM2-CAM-Zender), likely due to stronger soil moisture suppression in the Kok scheme (Li et al., 2022b). Similarly, the E3SM model produces less emissions from Asian sources when using the Kok scheme.~~

, but slightly decreases from 63% in E3SM2-Zender to 58% in E3SM3-Kok. The GISS-E2 models ~~exhibit minimal~~ show no differences in the regional ~~dust fractions between model versions (2.1 vs 2.2) and aerosol schemes (sectional OMA vs. modal MATRIX). However, total dust emissions are approximately~~ distributions. However, the total emission is about 40% lower when using ~~MATRIX compared to OMA, possibly due to differences in tuning parameters. Also, as noted in Bauer et al. (2022) , the MATRIX modal size distribution underrepresent~~ the MATRIX aerosol scheme. This could be due to different model tuning parameters, or underestimation of coarse dust particles (>5 μm diameter) ~~, which may contribute to lower emissions than OMA.~~

in the MATRIX modal size distribution, as pointed out by Bauer et al. (2022). UKESM1.0 simulates nearly twice as much dust as HadGEM3-GC3.1~~and~~ , along with slightly more even distributions. As described in Woodward et al. (2022), UKESM1.0 ~~produce similar spatial distributions but differ in global totals by more than a factor of two. UKESM1.0, which~~ is built on HadGEM3-GC3.1 ~~, uses the same dust scheme but includes several modifications that enhance the~~ but applies model tunings that enhance friction velocity and suppress ~~the topsoil moisturecontent, as described in Woodward et al. (2022). These parameter~~ soil moisture. These tunings are expected to increase the ~~surface gustiness and dryness, thereby enhancing the dust emission~~ wind gustiness and soil dryness in UKESM1.0~~. In addition, ~~ , thereby strengthening dust emissions. UKESM1.0 ~~excludes dust~~ also excludes emissions from seasonally vegetated ~~areas~~regions, resulting in smaller dust-emitting areas (Fig. 2p) compared to HadGEM3-GC3.1 ~~.~~

(Fig. 2o). The three Japanese models (MRI-ESM2.0, MIROC-ES2L, and MIROC6) exhibit large differences in total emissions and, to a lesser ~~extent~~degree, regional distributions. MRI-ESM2.0 produces ~~nearly double~~ similar regional fractions to JRAero but nearly twice the total emissions~~of JRAero, likely due to differences between assimilated and free-running meteorological data and in tuning parameters~~. Despite using the same dust scheme, MIROC-ES2L produces five times more

dust than MIROC6. This discrepancy ~~is largely driven by stronger near-surface~~ can be largely explained by the stronger winds in MIROC-ES2L~~. We find that the~~ , which produces 50% higher global mean wind speed ~~in MIROC-ES2L is about 50% higher than that in~~ than MIROC6. ~~Furthermore, the prescribed LAI in~~ Moreover, MIROC6 ~~is~~ prescribes non-zero LAI even in hyper-arid regions, which likely ~~contributes to lower emissions compared~~ further suppresses dust emissions relative to MIROC-ES2L (Hiroaki Tatebe, personal ~~communication~~communications).

~~Figure 3b shows the partitioning of global dust emissions by climate zones, providing a first-order assessment of model sensitivity to hydroclimate conditions. Dust emissions from hyperarid regions are expected to be primarily controlled by wind speed. These regions contribute 41% (INM-CM5.0) to 88% (CESM2-CAM-Kok) of global emissions across models. Contributions from arid/semiarid regions show greater variability, in the range of 8–37% and 0–18%, respectively. Among the ESMs, CanESM5.1, INM-CM5.0, and UKESM1.0 exhibit the highest semiarid contributions at 18%, 15%, and 12%, respectively. Overall, the model discrepancy increases with decreasing climate aridity, highlighting greater model uncertainty over the transitional areas between dry and humid climates. This pattern mirrors the relatively lower model spread for North Africa and the Middle East, as shown in Fig. 3a, where the predominance of hyperarid regions leads to stronger model agreement in dust emission attribution. Based on the model ensemble mean, global dust emissions are partitioned as 61% from hyperarid, 27% from arid, and 5% from semiarid zones. In comparison, MERRA2 (JRAero) produces 71% (65%), 26% (32%) and 3% (3%) of its global emissions from hyperarid, arid, and semiarid regions, respectively.~~

3.2 Interannual variability

~~In this section , we assess the degree of inter-model agreement~~ This section evaluates the consistency among the ESMs in simulating the interannual variability of dust emissions. Monthly dust emission fluxes from all ~~models are~~ ESMs are first regridded to a common ~~grid~~ resolution of 0.9°×1.25° ~~, and then deseasonalized by subtracting~~ (the native grid of CESM2). To remove the influence of annual cycles, we subtract the month-wise climatological ~~average at~~ means from each grid cell, yielding deseasonalized dust emission anomalies. Spearman's rank correlation coefficients are then ~~computed~~ calculated between the deseasonalized ~~dust flux anomalies for every possible pairwise comparison. With 23 datasets (i.e.,~~ anomalies for all possible model pairs. With 21 ESMs~~and 2 reanalysis products)~~, this yields ~~253 unique pairings~~210 pairwise comparisons. To quantify the ~~overall model~~ extent of inter-model agreement, we calculate the percentage of model pairs ~~exhibiting~~ that exhibit statistically significant (~~i.e.,~~ $p \leq 0.1$), positive correlations~~.~~ , which is displayed in Fig. 4. A higher percentage indicates stronger ~~model consensus in simulating dust interannual variability ; Conversely, low percentages indicate divergent dust variability. The results are displayed in Fig. 4.~~ inter-model agreement in simulating the interannual variability of dust emissions.

~~Overall, the models exhibit low to moderate agreement, with a maximum of 34% pairings exhibiting statistically significant, positive correlations. Despite being the world's largest sources, North Africa and the Middle East display poor~~ Despite its dominant contributions to global dust emissions, the hyperarid zone shows generally poor model agreement, with less than ~~12% of pairings yielding positive correlations, including over hotspot areas such as Bodélé Depression and Libyan Desert. This indicates that while global models consistently identify these regions as dominant dust sources, they differ substantially in simulating the year-to-year fluctuations. This poor agreement reflects model inconsistency in simulating the~~

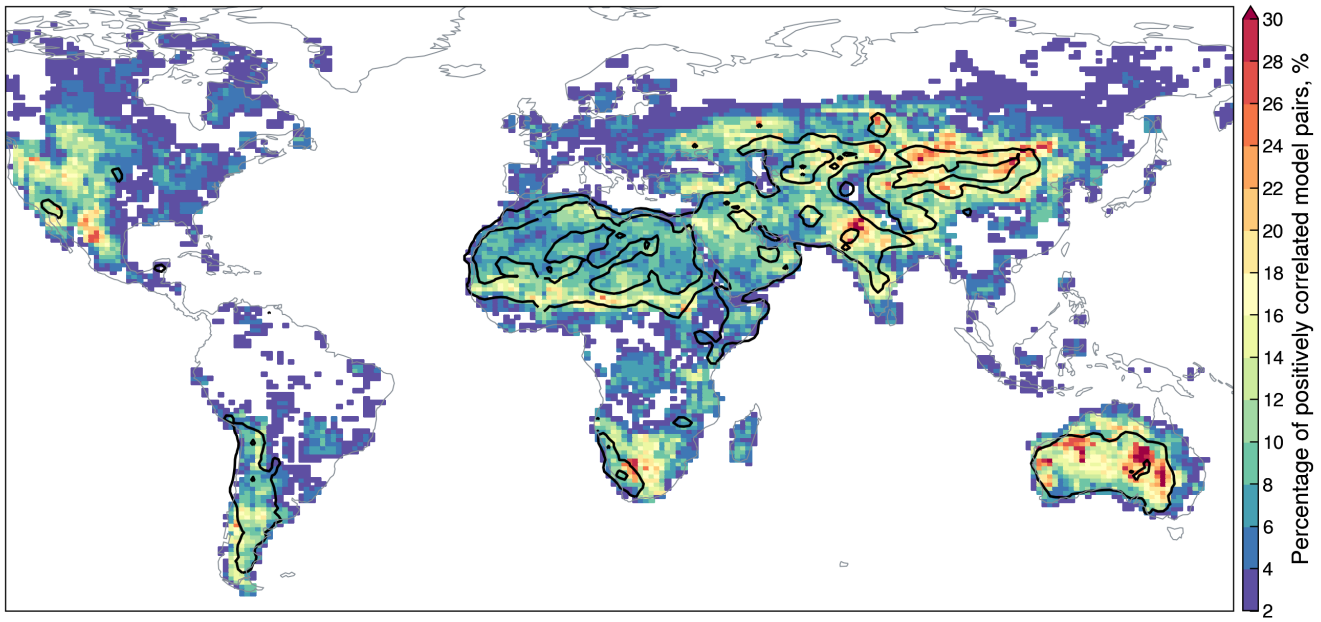

Figure 4. Percentage of statistically significant ($p \leq 0.1$), positive correlations out of every possible pairwise comparisons of monthly dust emission fluxes from ~~23 global~~ 21 Earth system models. Black contours represent the model ensemble mean annual dust flux of 10 and 100 Tg yr^{-1}.

~~near-surface wind speed, which is a predominant driver of dust emission from permanently dry, barren surfaces (Evan, 2018) . Interestingly, slightly better agreement is observed over the Sahel, where dust emission is more strongly modulated by hydroclimate conditions. Most other arid/semiarid regions show even better model agreement, indicating shared dust variability in regions where dust emission is strongly modulated by land cover and moisture availability, of which the influence on dust emission may be more consistently represented than wind extremes.~~

~~Spearman's rank correlation coefficients between global and regional monthly dust emission flux anomalies: (a) Global (GLB), (b) North Africa (NAF), (c) Southern Africa (SAF), (d) Middle East (MDE), (e) Central Asia (CAS), (f) South Asia (SAS), (g) East Asia (EAS), (h) North America (NAM), and (i) Australia (AUS). Dots indicate statistically significant correlations ($p \leq 0.1$). Summary tables are based on global models only (MERRA2 and JRAero not included).~~

~~Figure ?? presents the correlation matrix between global and regional averaged dust flux anomalies from individual models. The percentages of positive and negative correlations, and their ratio are calculated to provide an overall measure of model agreement for each region. Globally, the model intercomparisons yield 56% positive correlations and 44% negative correlations (Fig. ??a). Based on a significance level of $p \leq 0.1$, however, only 14% comparisons are strongly positively correlated and 7% negatively correlated, corresponding to an agreement-to-disagreement ratio of 1.9. The highest correlation is found between MERRA2 and JRAero, suggesting that assimilated meteorological and land surface conditions exert a strong, shared influence on the dust variability in reanalyses products. The consistency between MERRA2 and JRAero is also observed for individual~~

geographic regions (Fig. ??b–i). Among the ESMs, only CNRM-ESM2.1, UKESM1.0, and GFDL-ESM4 show significant correlations with either MERRA2 or JRAero, while other models exhibit either negative or insignificant relationships with the reanalyses. Particularly, MRI-ESM2.0 shows no significant correlation with JRAero, despite using the same dust scheme. The CESM, E3SM, and GISS-E2 model families show generally low internal agreement, with the best agreement found between E3SM2-Zender and E3SM3-Kok. Despite the common model heritage, poor agreement is found between UKESM1.0 and HadGEM3-GC3.1, and between MIROC6 and MIROC-ES2L10% of pairwise comparisons yielding statistically significant, positive correlations.

The model intercomparisons for individual regions are summarized below, focusing on statistically significant relationships between global models and reanalysis products, and within the CESM, E3SM and GISS-E2 model families:

(1) North Africa shows poor model agreement, with Because dust emissions from hyperarid areas are primarily controlled by wind speed, this weak agreement reflects inconsistent wind simulations in the ESMs. Indeed, we find that only 10% of pairings positively correlated, below the global average. Only GFDL-ESM4 and CESM2-CAM-Zender correlate with the reanalyses. NorESM2 is even negatively correlated with MERRA2. CESM, E3SM and GISS-E2 model variants exhibit weak or inconsistent internal correlations. model pairs produce statistically significant, positively correlated wind variability in the hyperarid zone. Similarly, Evan (2018) reported that dust-producing winds over the Sahara are mainly driven by large-scale meteorological processes and that most CMIP5 models failed to capture the near-surface wind variability. These results suggest that accurately representing near-surface winds is critical for reducing model discrepancies in dust variability over hyperarid areas.

(2) Southern Africa exhibits poor agreement, with only 8% positive correlations and an agreement-to-disagreement ratio of 1.1. CanESM5.1 is the only model positively correlated with MERRA2, while three models (MPI-ESM1.2

Based on the above analysis, hyperarid regions (e.g., North Africa and the Middle East) exhibit weak model agreementin the dust variability, whereas arid/semiarid regions tend to yield more coherent patterns. To further examine Compared to the hyperarid zone, arid and semiarid zones (such as the Sahel, South Asia, East Asia and Australia) exhibit significantly stronger model agreement. To illustrate how model consistency varies with hydroclimate conditionsclimate zones, Fig. 3.2 presents the pairwise correlation matrices of deseasonalized dust fluxes for based on dust flux anomalies averaged over hyperarid, arid, and semiarid climate zones. The proportion of positively correlated percentage of statistically significant, positively correlated model pairs increases from 10% in hyperarid regions the hyperarid zone to 14% in arid regions the arid zone and 17% in semiarid regions, indicating improved model agreement over the semiarid zone, indicating progressively higher model agreement in regions where dust emissions are more sensitive to increasingly influenced by hydroclimate and land surface conditions. However, semiarid regions also exhibit a greater number Meanwhile, the semiarid zone exhibits a larger percentage of negatively correlated model pairs (15%) than compared to hyperarid (5%) and arid (6%) regions. This dual pattern indicates zones. This dipole pattern suggests that as the climate regime transitions from hyperarid to semiarid, global models display increases in both consistency and divergence in the dust the ESMs exhibit both stronger agreement and worsened disagreement in simulating dust emission variability.

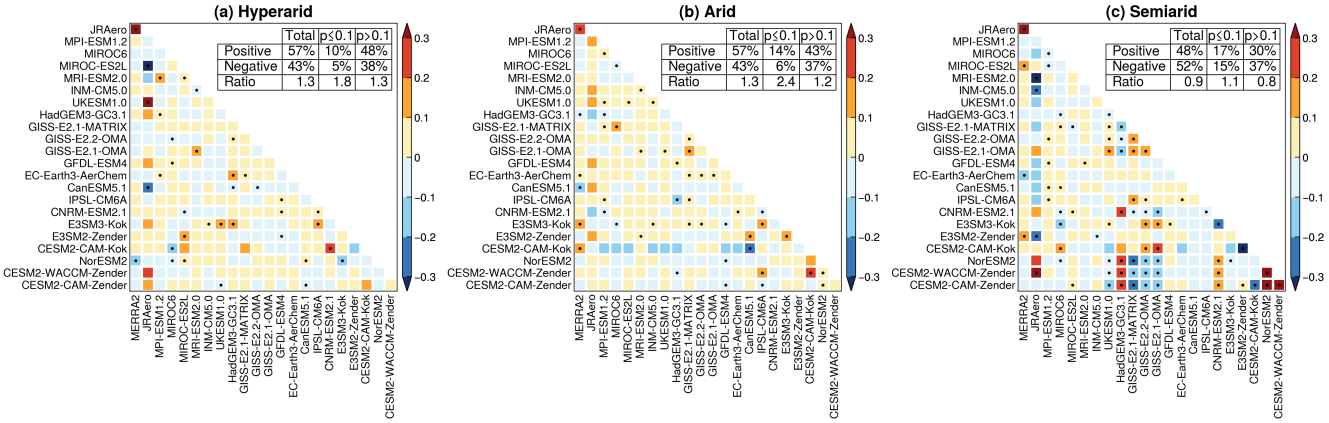

~~(3) Middle East shows similar model agreement to North Africa, with 12% positive correlations and an agreement-to-disagreement ratio of 1.9. MPI-ESM1.2 and E3SM2-Zender correlate with the reanalyses. Relationships within CESM, E3SM, and GISS-E2 models are mostly inconsistent, with positive correlation between CESM2-CAM-Zender and and CESM2-CAM-Kok only.~~

~~(4) Central Asia reports better model agreement, with 13% positive and an agreement-to-disagreement ratio of 3.1. E3SM3-Kok~~arid, ~~GISS-E2.1-MATRIX~~ and ~~CanESM5.1 yield modest agreement with the reanalyses. Only E3SM2-Zender and E3SM3-Kok are consistent within the families.~~

~~(5) South Asia exhibits the best model agreement, with 24% positively correlated pairings and an agreement-to-disagreement ratio of 6.2~~semiarid climate zones. ~~9 out of 19 models correlate with either MERRA2 or JRAero. GISS-E2 models show strong coherence. CESM2-CAM-Zender shows moderate corelation with CESM2-WACCM-Zender.~~

Dots indicate statistically significant correlations ~~(6) East Asia reports 10% positive correlations and the least (3%) negative correlations, with an agreement-to-disagreement ratio of 3.5. Six CMIP6 models are positively correlated with MERRA2. CESM and GISS-E2 families show moderate internal agreement.~~

~~(7) North America yields 12% positive correlations and an agreement-to-disagreement ratio of 2.3~~p≤0.1). ~~GISS-E2.1-MATRIX is the only model significantly correlated with the reanalyses. The CESM, E3SM, and GISS-E2 model families exhibit weak internal correlations.~~

Summary tables are based on Earth system models only ~~(8) Australia reports 12% positive correlations and an agreement-to-disagreement ratio of 2.9. Five CMIP6 models correlate with either~~ MERRA2 ~~or JRAero. GISS-E2 models show mixed results, with both positive and negative correlations. CESM2-CAM-Zender~~ and ~~CESM2-WACCM-Zender has strong agreement.~~

~~(9) South America exhibits poor model coherence, 10% positive correlations with an agreement-to-disagreement ratio of 1.5 (not shown). Only NorESM2 is strongly correlated with the reanalyses. CESM2-CAM-Zender shows modest agreement with CESM2-WACCM-Zender~~JRAero not included).

~~Same as Fig. **??** but for different climate zones.~~

~~(3) Middle East shows similar model agreement to North Africa, with 12% positive correlations and an agreement-to-disagreement ratio of 1.9. MPI-ESM1.2 and E3SM2-Zender correlate with the reanalyses. Relationships within CESM, E3SM, and GISS-E2 models are mostly inconsistent, with positive correlation between CESM2-CAM-Zender and and CESM2-CAM-Kok only.~~

~~(4) Central Asia reports better model agreement, with 13% positive and an agreement-to-disagreement ratio of 3.1. E3SM3-Kok~~arid, ~~GISS-E2.1-MATRIX~~ and ~~CanESM5.1 yield modest agreement with the reanalyses. Only E3SM2-Zender and E3SM3-Kok are consistent within the families.~~

~~(5) South Asia exhibits the best model agreement, with 24% positively correlated pairings and an agreement-to-disagreement ratio of 6.2~~semiarid climate zones. ~~9 out of 19 models correlate with either MERRA2 or JRAero. GISS-E2 models show strong coherence. CESM2-CAM-Zender shows moderate corelation with CESM2-WACCM-Zender.~~

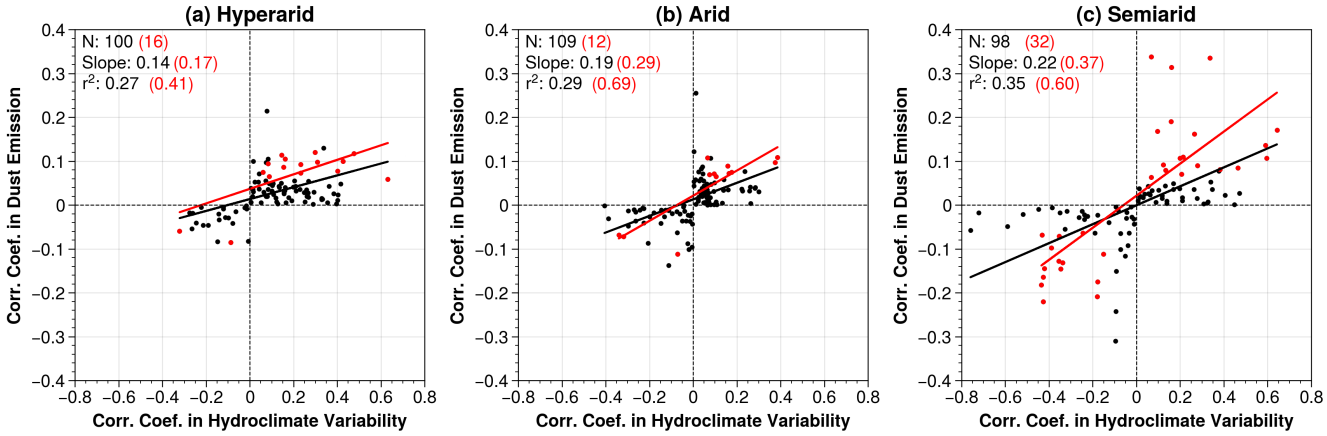

Figure 6. Statistical associations between the pairwise model correlation coefficients ($p \leq 0.1$ shown in red) in ~~deseasonalized~~ dust emission fluxes and hydroclimate variability ~~averaged~~ over (a) hyperarid, (b) arid, and (c) semiarid ~~regions~~climate zones. ~~Hydroclimate variability is represented by the first principle component (PC1) of five near-surface variables: precipitation, soil moisture, specific humidity, air temperature, and leaf area index.~~

What causes ~~such a~~ this complex behavior? ~~We hypothesize that model representations of the hydroclimate influence on dust emission play an important role. In semiarid regions~~ In semiarid environment such as temperate grasslands and ~~steppe ecosystems, dust emission is~~ steppes, dust emissions are strongly modulated by antecedent land surface conditions in addition to wind speed, such as ~~snow cover~~precipitation, soil moisture, and vegetation growth-decay cycle, which exert strong lagged ~~effects on dust activity in subsequent seasons (Shinoda et al., 2011; Nandintsetseg and Shinoda, 2015). Typically~~influence on the soil erodibility (Shinoda et al., 2011; Nandintsetseg and Shinoda, 2015). For example, dry anomalies during the prior wet season (e.g., ~~early snow retreat or reduced rainfall) may delay vegetation onset or~~ reduced snowfall or rainfall, accelerated snow retreat) can subsequently suppress vegetation growth, thereby ~~extending the duration of~~ prolonging bare soil exposure and ~~enhancing the soil erodibility~~increasing wind erosion risk. This delayed dust ~~response~~ emission response to preceding drought exemplifies the effect of land surface memory, ~~where persistent land surface conditions influence subsequent climate processes. Thus~~whereby the slow adjustment of land surface states (such as soil moisture, snow cover, and vegetation) over weeks to months influences subsequent dust emission long after the initial forcing (e.g., drought). Therefore, we speculate that the simultaneous increase ~~in model agreement and disagreement in semiarid regions (Fig. 3.2c)~~ of both model consistency and divergence from hyperarid to semiarid zones reflects a "double-edged sword" effect of land surface memory: models with coherent representations of hydroclimate variability ~~tend to converge in their dust emission responses~~ converge in the simulated dust emission variability (i.e., more positive correlations), while those with divergent hydroclimate representations ~~tend to diverge in dust responses~~ diverge in the dust variability (i.e., more negative correlations).

To ~~test~~ verify this hypothesis, we examine the statistical association between ~~inter-model~~ pairwise model correlations in dust ~~emission fluxes~~ emissions and those in hydroclimate ~~conditions~~variability. Specifically, we ~~perform~~ first perform a principle

component analysis (PCA) of ~~monthly-mean hydroclimate variables for each climate zone. The first~~ the five hydroclimate variables (i.e., precipitation, soil moisture, specific humidity, air temperature, LAI) for the hyperarid, arid, and semiarid zones. The leading principle component (PC1), which ~~accounts for~~ explains at least 40% of ~~total variances~~the total variance in all zones, is used ~~to represent~~ as a proxy for the dominant hydroclimate variability~~for each climate zone. Then, ~~. Spearman's rank correlation coefficients are ~~computed~~ then calculated for all pairwise model comparisons of deseasonalized monthly PC1 values, ~~similar to the dust flux comparisons~~ following the same approach as in Fig. 3.2.

~~Figure 6 displays the pairwise~~ Figure 6 compares the correlation coefficients for model pairs with ~~same-sign correlations in the dust flux and PC1~~ the same sign (i.e., either both positive or both negative) in dust emission fluxes and hydroclimate PC1. The regression slope and coefficient of determination (r^2) ~~hence~~ quantify the degree of statistical association between model ~~consistencies in the dust~~ correlations in dust emission and hydroclimate variability. The positive association ~~across~~ in all climate zones suggests that ~~models with stronger agreement in hydroclimate conditions~~ ESMs with stronger consensus in hydroclimate variability tend to produce more consistent dust variability, ~~while models that diverge in hydroclimate representations exhibit greater disagreement in dust variability. As the climate regime shifts from hyperarid to semiarid~~and vice versa. More importantly, both the number of ~~statistically significant model pairs and the~~ significantly correlated model pairs (N) and correlation strength (slope and r^2) ~~increase progressively, thus providing support for~~ show significant increases from hyperarid to semiarid zones. This result supports our hypothesis regarding the dual role of land surface memory: it enhances agreement among ~~models with coherent representations of hydroclimate dynamics~~ESMs with coherent hydroclimate representations, while simultaneously exacerbating disagreement among those with divergent hydroclimate variability. ~~This finding underscores the importance of accurately representing hydroclimate and land surface processes in reducing uncertainties in dust emission simulations, especially over transitional arid and semiarid regions.~~

3.3 Relative importance of wind and hydroclimate drivers

In this section, we present the dominance analysis ~~results on~~ of the collective and relative influence of wind and hydroclimate ~~variables~~ drivers on the dust ~~interannual variability within ESMs and MERRA2. Fig.~~ emission variability. Figure 7 presents the total variance explained (R^2~~explained by all predictors combined, representing the collective explanatory power of~~) by near-surface wind speed ~~,~~ and five hydroclimate variables (precipitation, soil moisture, specific humidity, air temperature, and LAI) in the ESMs and MERRA2. Results for CESM2-WACCM-Zender and NorESM2 are very similar to those of CESM2-CAM-Zender and thus not shown.

The ~~models~~ ESMs exhibit substantial differences in the total R^2, reflecting ~~varying degrees of~~ a large spread in the internal model variability and ~~differences in the~~ coupling strength between dust emission and ~~their physical drivers. Among the ESMs,~~ the six selected predictors. CanESM5.1 yields the lowest global R^2~~globally~~, followed by MPI-ESM1.2, MIROC6, and EC-Earth3-AerChem, ~~all of which show low R^2 values over extensive regions, suggesting that~~ in which the selected predictors explain ~~only a~~ a relatively small fraction of the ~~simulated dust variability in these models~~dust variability. The low ~~R~~explanatory power may be explained by several reasons. ~~For example, known model errors and artifacts~~ Specifically, model deficiencies and errors (e.g., in CanESM5.1, ~~as discussed in~~ Section 3.1~~, may distort or weaken~~) may weaken or distort the relationships

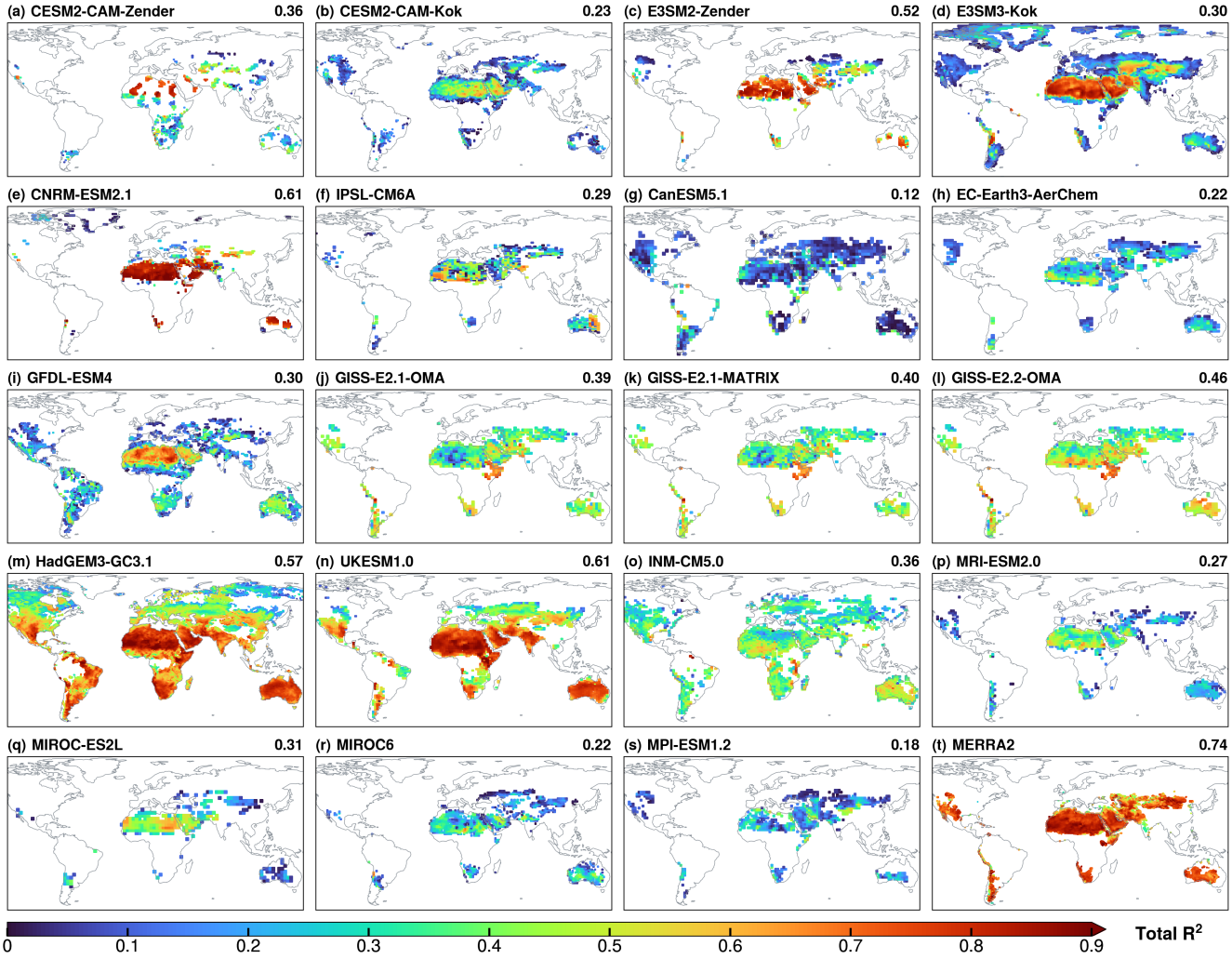

Figure 7. Total explained variance (R^2) in dust emission fluxes by six near-surface predictors (wind speed, precipitation, soil moisture, specific humidity, air temperature ~~,~~ and ~~leaf area index~~LAI) in ~~the deseasonalized monthly dust fluxes~~Earth system models and MERRA2. Global mean R^2 values are shown on each panel.

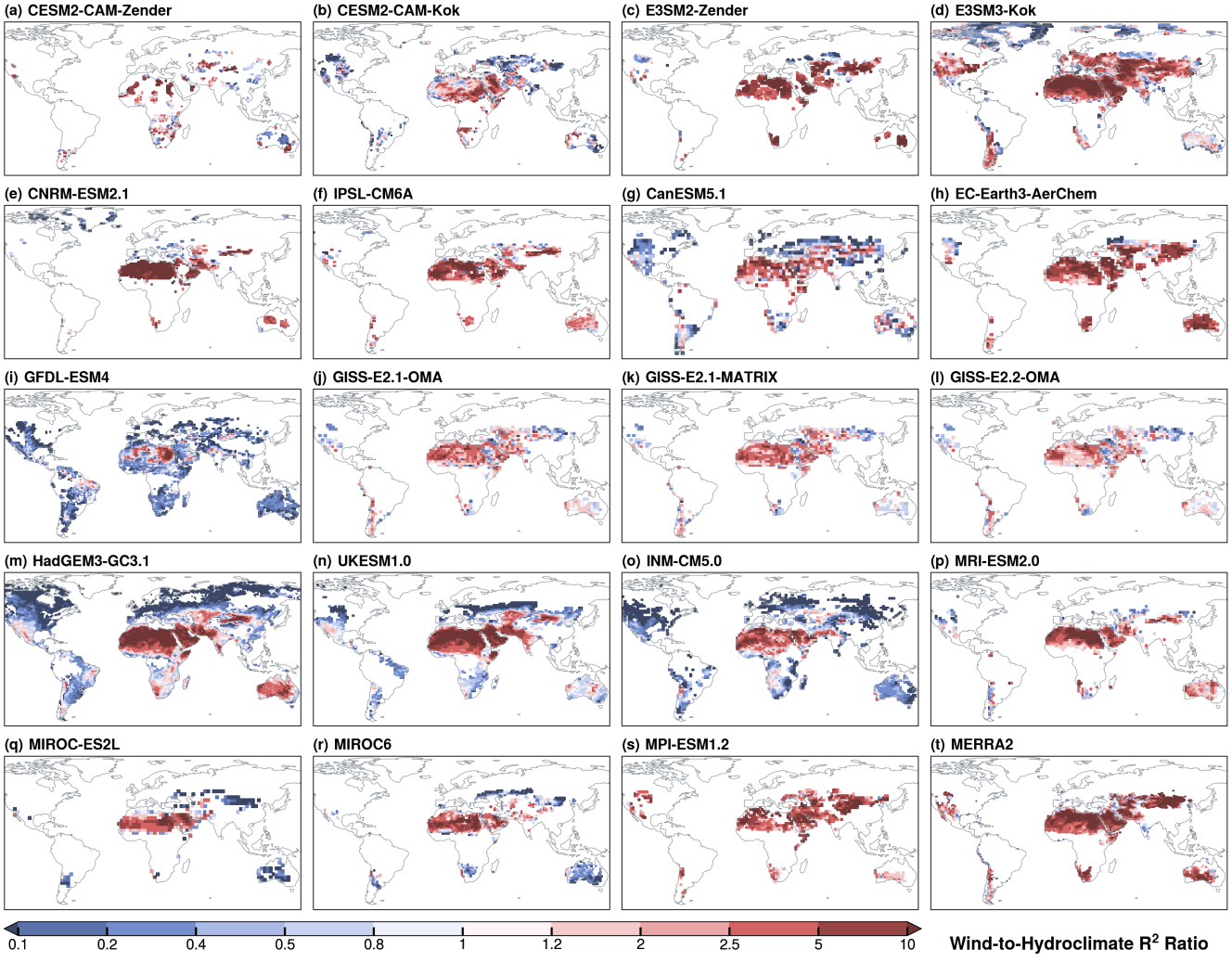

Figure 8. The ratio of ~~wind-associated~~ wind speed-associated R^2 to the combined R^2 of five hydroclimate variables (precipitation, soil moisture, specific humidity, air temperature ~~, leaf area index~~and LAI) in Earth system models and MERRA2.

between dust emissions and the ~~coupling between dust emission and its physical drivers. In models like INM-CM5.0, the~~ predictors. The use of over-simplified ~~dust parameterizations or reliance on time-invariant input fields~~ parameterizations and/or static land surface input (e.g., in INM-CM5.0) may weaken the dust–predictor relationship. In addition, dust emission ~~is inherently nonlinear and~~ involves inherently nonlinear processes and thus its relationship with the predictors may deviate from the linearity assumption in dominance analysis. As shown in Fig. 7, the total R^2 ~~is generally lowest over semiarid and subhumid regions, likely reflecting the~~ values tend to be much lower in arid and semiarid zones than in the hyperarid zone, likely due to increased nonlinearity between dust emission and hydroclimate variables which diminishes their collective explanatory power in a multilinear regression framework. Finally, the use of monthly ~~mean~~ model output, due to data availability, may dampen the short-term variability ~~in both dust fluxes and predictors, possibly weakening their statistical associations~~and statistical association between dust emission and the predictors.

Despite these limitations, most ~~models produce significant~~ ESMs produce significant total R^2 values ~~, indicating that the selected predictors capture a large portion of the simulated dust variability. This is particularly evident for North Africa and the Middle East, where the predictors explain over 60% of the total variance. Replacing the Zender dust scheme with Kok scheme generally leads to~~ over major source areas, especially in the hyperarid zone where the total R^2 exceeds 0.6. Switching from the Zender to Kok dust scheme leads to generally lower R^2 values in CESM ~~globally, and in~~ and E3SM ~~over most regions except Central and East Asia. In~~ (Fig. 7a–d). The GISS-E2 models ~~, switching the OMA and MATRIX microphysics schemesresults in minor changes in the total R^2, while the transition~~ show little differences between the OMA or MATRIX schemes, and a modest increase from version 2.1 to 2.2~~yields a modest increase~~. UKESM1.0 and HadGEM3-GC3.1 show minimal differences~~in total~~ , both with high R^2 values globally. MIROC6 yields ~~significantly~~ lower R^2 ~~values~~ than MIROC-ES2L, ~~particularly over hyperarid regions, likely due to differences in surface wind intensity and vegetation effects as discussed in Section 3.2. Compared to the ESMs,~~ especially over the hyperarid zone. MERRA2 ~~yields a higher global mean~~ produces higher R^2 than most ESMs, especially over ~~semiarid regions, highlighting the stronger dust–predictor relationships in the GOCART dust scheme with assimilated meteorological and land surface fields~~arid and semiarid zones. In summary, there are large spatial variability within individual ESMs and large inter-model discrepancies in the variance explained by the selected predictors.

~~Figure~~ To assess the relative importance of wind and hydroclimate drivers, Fig. 8 displays the ratio of ~~the~~ wind speed-associated R^2 to the combined R^2 of ~~hydroclimate variables, which indicate the relative importance of wind and hydroclimate drivers~~five hydroclimate variables. In all ESMs except GFDL-ESM4, the wind-to-hydroclimate R^2 ratio is well above 1 over ~~hyperarid regions, reflecting~~ the hyperarid zone, which is consistent with the dominant role of wind speed in ~~driving~~ controlling dust emissions from persistently dry, ~~bare~~ barren surfaces. In contrast, ~~the ratios exhibit large variability over~~ arid and semiarid ~~regions, with values both above and below 1.~~ zones exhibit greater discrepancies, with ratios either above or below 1 depending on the model. This reflects increased model ~~disagreement~~ discrepancies regarding the relative importance of wind and hydroclimate drivers in transitional ~~zones, where both factors interact more strongly and dust emission processes are more sensitive to~~ regions where dust emission is increasingly influenced by hydroclimate and land surface conditions.

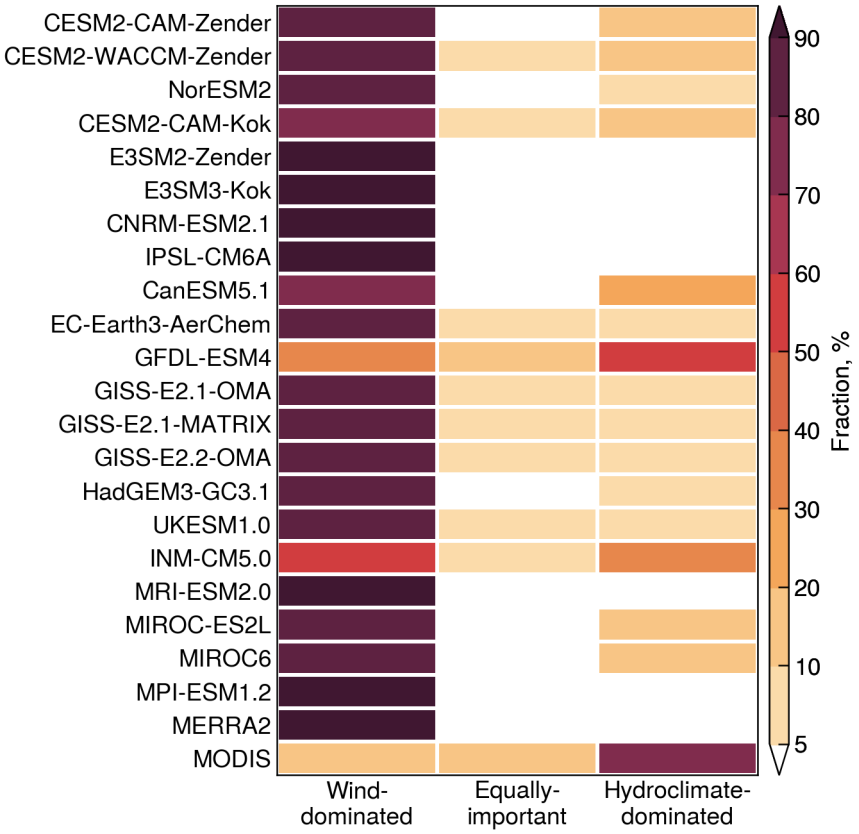

Figure 9. Fractional contributions of ~~three regimes (~~wind-dominated, equally-important, and hydroclimate-dominated ~~)~~ regimes to global dust emissions in ~~global~~ Earth system models and MERRA2.

Based on the wind-to-hydroclimate R^2 ratios, we classify global ~~dust source~~ dust-emitting areas into three regimes: wind-dominated (ratio>1.2), hydroclimate-dominated (ratio<0.8), and equally-important (0.8–1.2). ~~For each model, we~~ We then calculate the fractions of dust emissions originating from ~~each regime~~the three regimes in each model. The results are displayed in Fig. 9. The ESMs show general ~~consistency~~ agreement in the "equally-important" regime, with most models ~~simulating~~ producing less than 10% of ~~global dust emissions~~ dust from regions where wind and hydroclimate drivers have nearly equal ~~contributions~~influence on dust emissions. GFDL-ESM4 ~~yields~~ produces the highest contribution (12%) in this regime~~, while MERRA2 yields only 1%, lower than the ESMs~~.

~~MERRA2 and most ESMs simulate more than 80% of dust emissions from the~~ The wind-dominated ~~regime~~regime contributes the majority of global dust emissions (>80%) in most ESMs and MERRA2, consistent with the dominant ~~role of permanently dry, barren areas in global dust production.~~ contribution of the hyperarid zone (Fig. 3). However, three models ~~deviate from this pattern.~~ yield anomalously low contributions: GFDL-ESM4 ~~and~~ (36%), INM-CM5.0 ~~simulate less than 60% of emissions from wind-dominated regions, while~~ (54%) and CanESM5.1 ~~yields a moderately lower fraction of~~ (75%~~. Correspondingly, these~~

models exhibit significantly higher fractions from the hydroclimate-dominated regime. The anomalous emission partitioning in these models may). These deviations can be explained by different reasons. In As shown in Fig. 3, INM-CM5.0 and CanESM5.1 , the relatively balanced distribution may result from their homogeneous dust emission patterns, likely due to the model limitations or biases discussed in Section 3.2. In contrast, the behavior of produce relatively spatially homogeneous emission pattern, which explains the lower contributions from hyperarid or wind-dominated areas. In comparison, the low estimate in GFDL-ESM4 is driven by due to the model's anomalously strong hydroclimate influence over hyperarid regionsthe hyperarid zone. As shown in Fig. 8i, GFDL-ESM4 exhibits heterogeneous markedly low wind-to-hydroclimate R^2 ratios , with counterintuitively large fractions of the dust variability attributed to hydroclimate drivers over West Africa, the Middle Eastratios (<1) over North Africa, Arabian Peninsula, and Iranian Plateau.

, which are consequently misclassified into the hydroclimate-dominated regime. These regions are characterized by scarce precipitation and very low hydroclimate variability, which is expected to have negligible influence on dust emissions. For CESM and E3SMmodels, switching from the Zender to Kok dust scheme reduces the proportion of dust emissions from slightly reduces the wind-dominated regionsdust fraction: from 85% to 80% in CESM, and from 99% to 96% in E3SM. These changes suggests that the Kok scheme, which incorporates more physically-based representations of soil erodibility, allocates a larger share of emissions to transitional regions. The GISS-E2 models show minimal differences between model versions or aerosol schemes, within the range of yield similar estimates regardless of model version or aerosol scheme, with 82–85% dust from the wind-dominated regime. Similarly, UKESM1.0 and HadGEM3-GC3.1 produce identical yield similar estimates, with 90% of emissions dust emitted from wind-dominated regions. MERRA2 simulates 98% emissions from the wind-dominated regime, higher than most ESMs.

Fig. 9 The above analysis not only confirms the anomalous dust spatial emission patterns in CanESM5.1 and INM-CM5.0 (as seen as previously shown in Fig. 3), but also identifies GFDL-ESM4 as an outlier in representing the relative influence of wind and hydroclimate drivers. To further assess the model consistency in predictor importance, we calculate the fractional due to its misrepresentation of predictor relative importance. Here we further evaluate the contribution of wind speed to the total R^2 over hyperarid, arid, and semiarid zones. The grid-level distributions of wind-associated in different climate zones. For each climate zone, we use ridgeline plots to illustrate the statistical distributions of grid-level wind speed-associated R^2 fractions. The results are displayed in Fig. 10. A median In the ridgeline plots, if the median value of wind speed-associated R^2 fraction fractions (denoted by a red vertical line in Fig. 10) is above 50%indicates that wind speed contributes to more than , it means wind speed dominates the dust variability at more than half of the grid cells. If the median value is below 50%of the simulated dust variability at , the dust variability is dominated by hydroclimate drivers at more than half of the grid cells.

In hyperarid regions, the hyperarid zone (Fig. 10a), most ESMs and MERRA2 and most ESMs exhibit dominant wind controlscapture the dominant control of wind speed, with the median wind R^2 fraction fractions exceeding 80%. The three GISS-E2 models show slightly reduced wind influence similar spatial variability, with slightly lower median values (∼70%). In contrast, Two models stand out as notable outliers: GFDL-ESM4 and CESM2-CAM-Kokexhibit significantly lower wind influence and greater spatial variability , both of which exhibit large variability and low median values. In particular, GFDL-ESM4 yields a median wind R^2 fraction of 42%, indicating that half of the grid cells are dominated by hydroclimate drivers

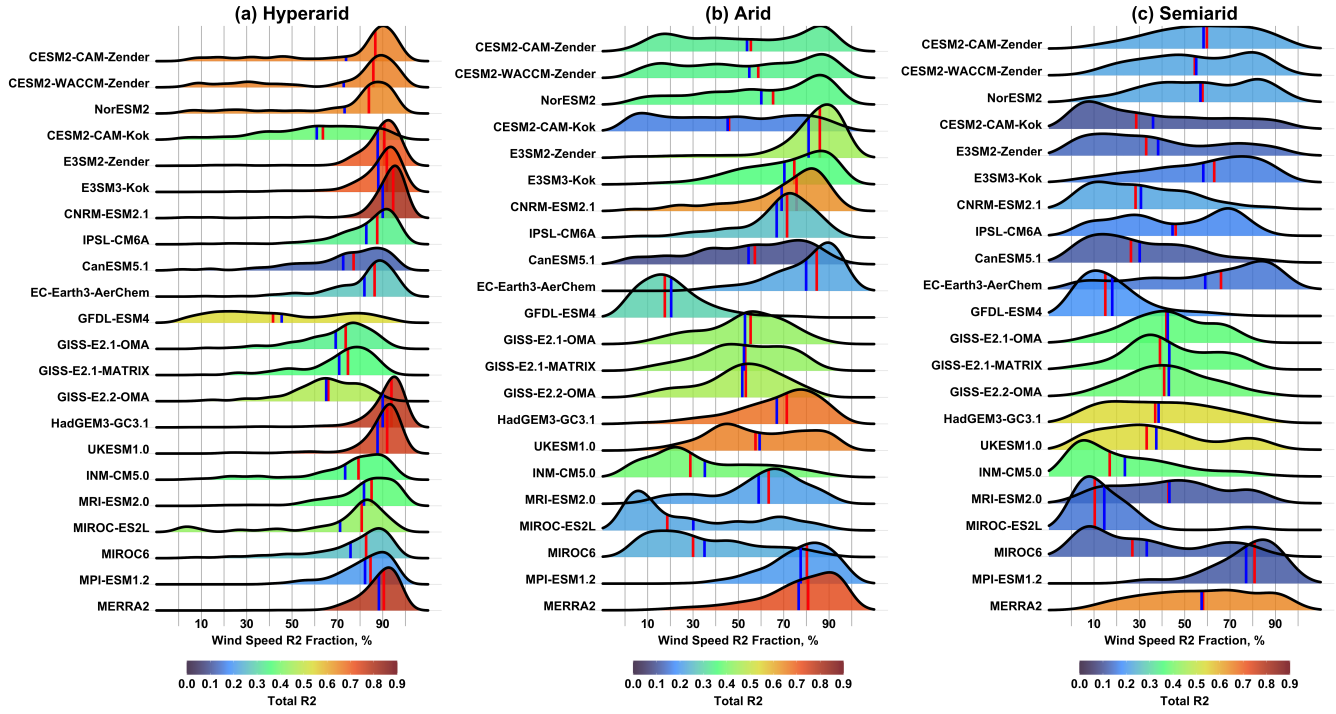

Figure 10. Ridgeline plots of ~~grid-level~~ the fractional contributions of wind speed to the total R^2 over (a) hyperarid, (b) arid, and (c) semiarid ~~regions~~climate zones. ~~Red (blue) vertical lines indicate~~ The median ~~(~~and mean ~~)~~ values are denoted by red and blue vertical lines, respectively. Color shading represent the mean total R^2 ~~of all predictors~~values.

~~. Within the CESM family, the choice of CAM vs. WACCM modules has a minimal effect, both yielding~~ an overestimated sensitivity to hydroclimate drivers in the hyperarid zone, particularly over North Africa, Arabian Peninsula and Iranian Plateau (Fig. 8i). Similarly, CESM2-CAM-Kok exhibits large spatial variability with a median wind R^2 fraction of 64%, driven by dominant hydroclimate influence over West Africa and the Tarim Basin (Fig. 8b). In comparison, CESM2-CAM-Zender captures the dominant wind influence with a median value of 86%. ~~However, replacing the Zender dust scheme with the Kok scheme significantly reduces the total R^2 and wind influence (64%) while increasing the spatial variability. These differences persist even~~ The suboptimal performance of CESM2-CAM-Kok relative to CESM2-CAM-Zender persists when comparing common ~~dust-emitting areas , suggesting that the changes are driven by different model physics in the Zender and Kok schemes. Conversely, switching from Zender to Kok in E3SM yields negligible changes in total R^2 or wind contributions. GISS-E2 modelsshow broad similarity between the OMA and MATRIX aerosol schemes, with a slight reduction in wind R^2 fraction in version 2.2 relative to version 2.1~~dust-producing areas in the two models.

~~Compared to hyperarid regions, the ESMs show generally lower~~ In the arid zone (Fig. 10b), the total R^2 ~~over arid regions, indicating~~ is generally smaller due to reduced explanatory power of the ~~selected predictors. Wind speed remains the dominant driver in most models, though its influence~~ predictors. The ESMs also show larger disagreement in the relative importance of

wind and hydroclimate drivers. The influence of wind speed is reduced and ~~becomes more spatially heterogeneous. CESM2-CAM-Kok shows increased variability in the wind R^2 fraction with a median value of 46%, compared to 64% in hyperarid regions. Four~~ more variable, but still remains dominant in most ESMs and MERRA2. The GISS-E2 models produce relatively equal importance of wind and hydroclimate drivers. In contrast, four models—GFDL-ESM4, INM-CM5.0, MIROC-ES2L and MIROC6—yield ~~a~~ dominant hydroclimate influence with the median wind R^2 fraction falling well below 50%, indicating a transition from wind- to hydroclimate-dominated regimes. ~~In~~ CESM2-CAM-Kok also reflects this transition, with a median value of 46%. In both CESM and E3SM, switching from the Zender to Kok ~~schemes reduces the wind dominance, possibly because physically-based~~ scheme results in weaker wind and stronger hydroclimate influences, likely due to the physically based soil erodibility treatment in ~~Kok~~ the Kok scheme which enhances the dust sensitivity to hydroclimate ~~variables, as suggested previously (Kok et al., 2014a)~~variability, as previously suggested in Kok et al. (2014a).

~~In semiarid regions, the influence of wind speed further declinesas the hydroclimate influence strengthens in all models~~Results for the semiarid zone (Fig. 10c) are considered less robust due to significantly smaller dust-emitting areas or model grid cells (Fig. 1). In general, the wind influence further declines, while hydroclimate divers become more important. The magnitude ~~and spatial pattern of this change~~of this shift, however, ~~vary considerably~~varies widely, leading to ~~large model disagreement in the relative importance of wind and hydroclimate drivers~~larger discrepancies. Specifically, ~~the hydroclimate dominance is further strengthened~~ hydroclimate drivers continue to dominate in CESM2-CAM-Kok, GFDL-ESM4, INM-CM5.0, MIROC-ES2L and MIROC6, ~~and MIROC-ES2L. Five models—E3SM2-Zender~~same as in the arid zone. The following ESMs display a clear transition to hydroclimate-dominated regimes: E3SM2-Zender, CNRM-ESM2.1, CanESM5.1, HadGEM3-GC3.1, and UKESM1.0~~—shift from wind- to hydroclimate-dominated regimes. The rest of ESMs (especially MPI-ESM1.2)~~. IPSL-CM6A and GISS-E2 models also show increased hydroclimate influence, though to a lesser extent. The remaining ESMs and MERRA2 continue to ~~maintain wind dominance~~ display dominance of wind speed, albeit with ~~reduced wind R^2 fraction and~~ increased spatial variability. ~~Interestingly, implementing the Kok dust scheme in CESM and E3SM produces different impacts: it reduces (enhances) the wind influence in CESM (E3SM) compared to the Zender scheme. GISS-E2 models display very similar patterns between aerosol schemes and model versions in both arid and semiarid zones.~~

The above analysis ~~identifies~~ indicates that GFDL-ESM4 and CESM2-CAM-Kok ~~as notable outliers in hyperarid regions, due to the anomalously strong influence of hydroclimate drivers in the two models. To investigate the source of this influence~~simulate anomalously strong hydroclimate influence in the hyperarid zone. To identify the specific drivers of these anomalies, Fig. 11 presents the median fractional contributions of ~~individual~~ five hydroclimate variables to the total R^2~~across different climate zones. Over hyperarid regions,~~ . In the hyperarid zone, most ESMs capture the negligible sensitivity of dust emission to hydroclimate variables. Several exceptions exist, however. CESM2-CAM-Kok ~~exhibits anomalous contributions~~ shows unusually strong influence from precipitation and specific humidity~~to the simulated dust variability. These influences further strengthen over arid and semiarid regions. In contrast,~~ , while GFDL-ESM4 exhibits ~~strong influence from soil moisturein hyperarid regions, and from LAI in arid and semiarid regions. Additionally, the~~ anomalously strong sensitivity to soil moisture. The GISS-E2 models display ~~strong sensitivities~~ moderately elevated sensitivity to soil moisture and specific humidity, which ex-

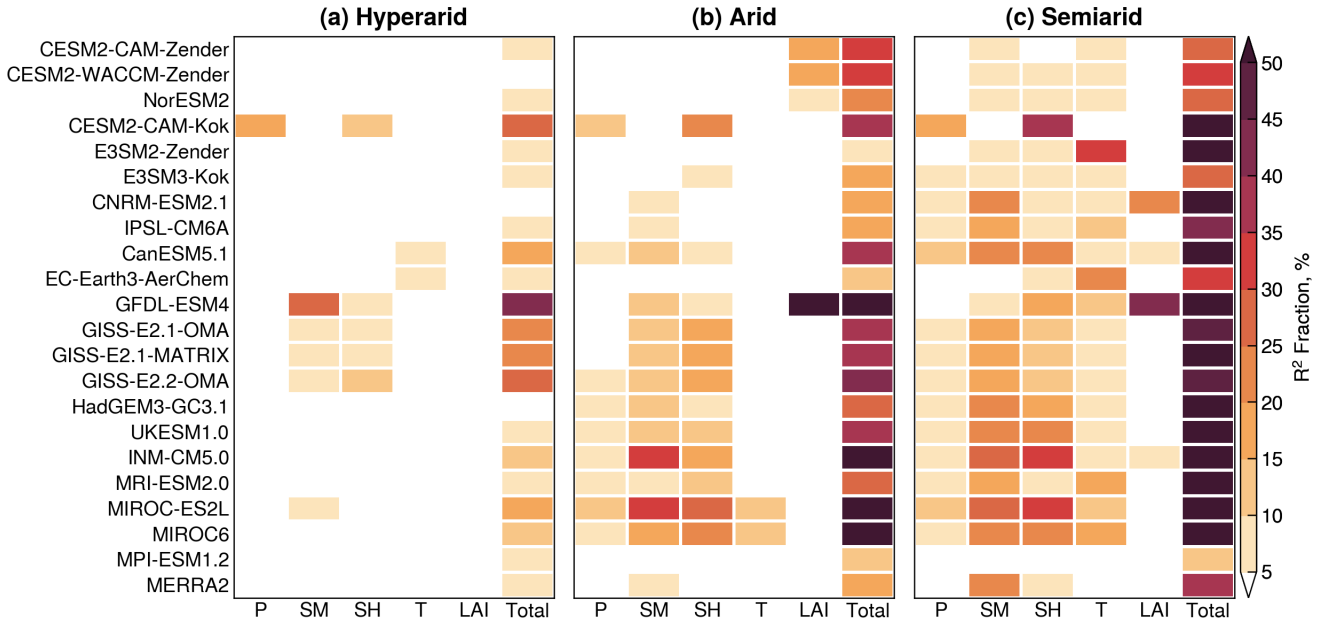

Figure 11. Median factional contributions of hydroclimate variables to the total explained variance (R^2) in ~~individual~~ Earth system models and MERRA2 over (a) hyperarid, (b) arid, and (c) semiarid ~~regions~~climate zones. ~~The hydroclimate~~ Hydroclimate variables are precipitation (P), soil moisture (SM), specific humidity (SH), air temperature (T), and leaf area index (LAI).

plains their moderate wind ~~dominance in hyperarid regions~~ influence in the hyperarid zone (Fig. 10a). ~~These anomalously strong sensitivities to hydroclimate variables help explain the reduced wind control in these models.~~

The overestimation of hydroclimate influence in the hyperarid zone may be explained by a combination of two mechanisms: (1) the hydroclimate variability is overestimated in the model, which induces spurious effects on dust emissions; or (2) the hydroclimate variability is reasonably captured, but the dust scheme incorporates overly strong sensitivity to hydroclimate drivers. Shevliakova et al. (2024) reported that the GFDL-ESM4 land model significantly overestimates soil moisture over dryland regions, with values more than double those from satellite observations in dust source regions like the central Sahara and Tarim Basin. This bias likely explains the strong apparent sensitivity of dust emission to soil moisture in GFDL-ESM4 (Fig. 11a).

The abnormal hydroclimate influence in CESM2-CAM-Kok may be partly explained by dust emission parameterizations in the Kok scheme, which introduces enhanced sensitivity to the threshold wind velocity compared to the Zender scheme (Kok et al., 2014a). Because of this heightened dependence on land surface conditions, the Kok scheme does not require predefined dust source functions and is considered more physically realistic for projecting dust responses to future climate and land-use changes. Another possible reason is the relatively short simulation period in CESM2-CAM-Kok (2004–2013), which may not fully capture the long-term variability and predictor influence as in CESM2-CAM-Zender (1980–2014). In this regard, the E3SM experiments provide a more robust comparison between the Zender and Kok schemes. As shown in Fig.

11a, the E3SM models exhibit negligible hydroclimate influence in the hyperarid zone, regardless of the dust scheme used. In the arid zone, however, E3SM3-Kok shows higher hydroclimate influence than E3SM2-Zender due to increased sensitivity to specific humidity (Fig. 11b). This comparison provides additional evidence that the Kok scheme amplifies the dust emission sensitivity to hydroclimate conditions.

In the arid zone (Fig. 11b), most ESMs show enhanced influence from soil moisture and specific humidity, consistent with empirical evidence that both variables strongly affect the soil erodibility and wind erosion risk (e.g., Csavina et al., 2014; RAVI et al., 2006; . Interpreting the LAI influence, however, is more complex due to several factors. First, unlike other hydroclimate variables, LAI can be either prescribed from climatology or simulated by the model's dynamic vegetation component (Table 1). Models using prescribed LAI are expected to show minimal interannual variability and hence limited influence on dust emissions. Second, the LAI effect on dust emission is treated differently. For example, CESM assumes a linear relationship between bare soil fraction and LAI when LAI is below 0.3, while GFDL-ESM4 assumes an exponential decrease in bare soil fraction as a function of LAI. Because LAI is often used to derive bare soil fraction in vertical dust flux calculations, these differences can alter the modeled dust sensitivity to vegetation cover. Most ESMs in Fig. 11b exhibit weak to negligible LAI influence, likely reflecting either prescribed LAI or the normalization of dust fluxes prior to dominance analysis (see Section 2). One outlier is GFDL-ESM4 which exhibits the strongest sensitivity to LAI, even well above the sensitivity to soil moisture. This can be explained by the strong coupled between LAI and dust emission in the model, and the fact that no normalization was applied to GFDL-ESM4 due to missing bare soil fraction output from the CMIP6 archive.

4 Conclusions

~~This study evaluates the climatological distribution and interannual variability of historical dust emission fluxes simulated by~~

This study evaluates discrepancies and biases among 21 ~~ESMs and two reanalysis products (MERRA2 and JRAero)across major geographic regions and climate zones (hyperarid, arid, and semiarid). Using the dominance analysis technique, we quantify the collective and relative influence~~ ESMs in representing the interannual variability of windblown dust emissions and the relative importance of near-surface wind speed and hydroclimate ~~variables (i.e.,~~ drivers (precipitation, soil moisture, specific humidity, air temperature, and LAI)~~in modulating the dust interannual variability. By treating dust emission as a~~ . We treat dust emission flux as an unobservable, model-specific quantity ~~shaped by the internal variability and physical parameterizations within individual models, this study provides new insights into the consistencies, divergences, and potential biases~~ and use dominance analysis to quantify the variance explained in dust emission fluxes by wind and hydroclimate drivers within each model. The analysis is conducted over three climatologically defined climate zones (hyperarid, arid, and semiarid), and further examines the effect of dust emission ~~representations in ESMs.~~ parameterizations through paired CESM and E3SM experiments with the Zender et al. (2003) and Kok et al. (2014b) schemes.

~~Substantial inter-model spread is observed in global dust emission totals and their regional distributions, consistent with previous analyses of AEROCOM and CMIP5 experiments. While most models identify North Africa and the Middle East as the dominant dust source,~~ The hyperarid zone contributes more than half of global dust emissions in all models except CanESM5.1

and INM-CM5.0simulate significantly lower contributions from these regions, possibly , which simulate relatively spatially even emission patterns with less than 50% from the hyperarid zone, likely due to known model errors and limitations (e.g., over-simplified dust parameterizations). Furthermore, models exhibit poor agreement in simulating the interannual variability of dust emissions, especially over hyperarid regions (such as North Africa and the Middle East). Despite their dominant global contributions, hyperarid regions exhibit poor model agreement in the deseasonalized monthly dust fluxesdeficiencies and over-simplifications in dust emission representations. In the hyperarid zone, the ESMs exhibit poor agreement with each other and with MERRA2 in simulating the dust variability, with only 10% of the pairwise model comparisons yielding statistically significant, positive correlations. This reflects inconsistent model representations of near-surface winds, which is a primary controlling factor of dust emissions from permanently dry, barren surfaces. Indeed, most models capture the dominant control of wind speed in hyperarid regions, with a few exceptions. Specifically, GISS-E2 models show slightly lower wind influence (~70%) due to elevated contributions from soil moisture and specific humidity. Two models emerge as important outliers: GFDL-ESM4 and CESM coupled with the Kok et al. (2014b) dust scheme, which exhibit significantly lower wind influence and greater spatial variability, due to anomalous sensitivities to soil moisture and precipitation/specific humidity, respectively.

In arid and semiarid regions where dust mobilization is increasingly modulated by vegetation and water availability, model behavior becomes more complex, with both increased consistency and inconsistency in the dust interannual variability. An empirical analysis reveals that this behavior is caused by a dual zones, the ESMs exhibit a dipole pattern with both improved agreement and increased disagreement. This behavior can be explained by a "double-edged sword" effect of land surface memory: models with coherent representations of hydroclimate variability tend to converge in their dust emission responsesvariability, while those with divergent hydroclimate representations tend to diverge in dust variability. As a result, models exhibit increased spatial variability and spread in predictor importance. Specifically, while all models capture the progressive increase of hydroclimate influence with decreasing aridity, the magnitude and spatial pattern of this transition vary considerably, leading to increased inconsistency on the dominant dust emission driver (i.e., wind speed vs. hydroclimate). These findings underscore major model uncertainties in the emission responses.

The relative influence of wind and hydroclimate drivers also varies with climate regimes. Most ESMs capture the dominant control of wind speed and weak sensitivity to hydroclimate conditions in the hyperarid zone, except CESM2-CAM-Kok and GFDL-ESM4, both of which show great spatial variability and abnormally strong influence from precipitation, specific humidity, and soil moisture. The overestimated hydroclimate influence in GFDL-ESM4 can be explained by the model's overestimation of soil moisture and consequent spurious effects on dust emissions. The enhanced hydroclimate influence in CESM2-CAM-Kok (relative to CESM2-CAM-Zender) may be explained, at least partly, by the physically based soil erodibility formulations in the Kok et al. (2014b) scheme, which replaces the use of predefined dust sensitivity to underlying physical drivers over transitional environment.

The effects of replacing the Zender et al. (2003) dust scheme with the new Kok et al. (2014b) scheme in CESM and E3SM are also examined. In CESM, the Kok et al. (2014b) scheme yields stronger hydroclimate influence and larger spatial variability across all climate zones, likely due to its more physically-based treatment of soil erodibility and reduced reliance on static dust source functions. Other possible causes include inconsistent dust emitting areas and dust radiative feedback treatments.

In A similar pattern is found in E3SM, switching from Zender to Kok scheme yields mixed responses depending on the climate zone: negligible change over hyperarid regions, enhanced hydroclimate influence over arid regions, and enhanced wind where switching from the Zender et al. (2003) to the Kok et al. (2014b) scheme strengthens the hydroclimate influence over semiarid regions. These results suggest that the inherent dust sensitivity to climate variations may depends on both the dust emission parameterization and the host modelin the arid zone. However, due to concurrent updates in model physics (e.g., dust mineralogy, radiative feedbacks, and meteorology), further experiments are needed to isolate the effects of dust emission parameterizations on dust–climate sensitivities.

In arid and semiarid zones, the influence of wind speed generally weakens while the hydroclimate influence strengthens. However, the relative importance of wind and hydroclimate drivers becomes increasingly inconsistent between the models, with an increasing number of ESMs shifting toward comparable or dominant-dominated regimes. In general, MERRA2 produces stronger wind influence and weaker hydroclimate influence than the ESMs.

In summary, this study highlights substantial inconsistencies in how global models represent dust emission variability and its physical drivers . While most models provides new insights into how ESMs represent the temporal variability and physical drivers of windblown dust emissions. Most ESMs capture the dominant role of wind control over permanently dry, barren surfaces, their poor agreement in dust variability highlights large inconsistencies in the simulated near-surface windsin hyperarid regions, there is considerable divergence in transitional areas, where hydroclimate . The dipole model behavior in arid and semiarid zones underscores the important role of hydroclimate variability and land surface processesplay increasingly important roles. Improving model representations of soil and vegetation dynamics and dust-climate relationships interactions in these regions is essential for reducing uncertainties in predicting dust responses to climate variations and changefuture projections of dust emissions under changing climate and land-use conditions.

Data availability. Model comparison and dominance analysis results are available at https://doi.org/10.5281/zenodo.15741734.

Author contributions. XX designed this study with input from LL. XX and XL performed the analysis and wrote the initial manuscript. LL performed CESM2-CAM-Kok simulations. YF performed E3SM simulations. All authors edited the manuscript.

Competing interests. The authors declare no competing interests.

Acknowledgements. X.L. and X.X. are partly partially supported by the NASA Land-Cover and Land-Use Change Program. Y.F. acknowledges the support of the Energy Exascale Earth System Model (E3SM) project, funded by the U.S. Department of Energy (DOE), Office of Science, Office of Biological and Environmental Research. The work at Argonne National Laboratory was supported by the U.S. DOE Office of Science under contract DE-AC02-06CH11357. L.L. acknowledges support from the U.S. Department of Energy (DOE) under

award DE-SC0021302, and from the Earth Surface Mineral Dust Source Investigation (EMIT), a National Aeronautics and Space Administration (NASA) Earth Ventures-Instrument (EVI-4) mission. He also acknowledges the high-performance computing resources provided by Derecho at the National Center for Atmospheric Research (NCAR), through NCAR's Computational and Information Systems Laboratory (CISL), which is sponsored by the National Science Foundation (NSF). The authors acknowledge the World Climate Research Programme for coordinating and promoting CMIP6, and thank the climate modeling groups for producing and making available their model output, the Earth System Grid Federation (ESGF) for archiving the data and providing access, and the multiple funding agencies who support CMIP6 and ESGF.

References

Albani, S., Mahowald, N. M., Perry, A. T., Scanza, R. A., Zender, C. S., Heavens, N. G., Maggi, V., Kok, J. F., and Otto-Bliesner, B. L.: Improved dust representation in the Community Atmosphere Model, Journal of Advances in Modeling Earth Systems, 6, 541–570, https://doi.org/10.1002/2013MS000279, 2015.

Aryal, Y. and Evans, S.: Dust emission response to precipitation and temperature anomalies under different climatic conditions, Science of the Total Environment, 874, https://doi.org/10.1016/j.scitotenv.2023.162335, 2023.

Aryal, Y. N. and Evans, S.: Global Dust Variability Explained by Drought Sensitivity in CMIP6 Models, Journal of Geophysical Research: Earth Surface, 126, https://doi.org/10.1029/2021JF006073, 2021.

Azen, R. and Budescu, D. V.: The Dominance Analysis Approach for Comparing Predictors in Multiple Regression, Psychological Methods, 8, 129–148, https://doi.org/10.1037/1082-989X.8.2.129, 2003.

Balkanski, Y., Schulz, M., Claquin, T., Moulin, C., and Ginoux, P.: Global Emissions of Mineral Aerosol: Formulation and Validation using Satellite Imagery, in: Emissions of Atmospheric Trace Compounds, edited by Granier, C., Artaxo, P., and Reeves, C. E., pp. 239–267, Springer, https://doi.org/10.1007/978-1-4020-2167-1_6, 2004.

Bauer, S. E., Tsigaridis, K., Faluvegi, G., Nazarenko, L., Miller, R. L., Kelley, M., and Schmidt, G.: The Turning Point of the Aerosol Era, Journal of Advances in Modeling Earth Systems, 14, https://doi.org/10.1029/2022MS003070, 2022.

Bergametti, G., Marticorena, B., Rajot, J. L., Chatenet, B., Féron, A., Gaimoz, C., Siour, G., Coulibaly, M., Koné, I., Maman, A., and Zakou, A.: Dust Uplift Potential in the Central Sahel: An Analysis Based on 10 years of Meteorological Measurements at High Temporal Resolution, Journal of Geophysical Research: Atmospheres, 122, 433–12, https://doi.org/10.1002/2017JD027471, 2017.

Bryant, R. G.: Recent advances in our understanding of dust source emission processes, Progress in Physical Geography, 37, 397–421, https://doi.org/10.1177/0309133313479391, 2013.

Budescu, D. V.: Dominance analysis: A new approach to the problem of relative importance of predictors in multiple regression, Psychological Bulletin, 114, 542–551, https://doi.org/10.1037/0033-2909.114.3.542, 1993.

Bullard, J. E., Harrison, S. P., Baddock, M. C., Drake, N., Gill, T. E., McTainsh, G., and Sun, Y.: Preferential dust sources: A geomorphological classification designed for use in global dust-cycle models, Journal of Geophysical Research: Earth Surface, 116, https://doi.org/10.1029/2011JF002061, 2011.

Cakmur, R. V., Miller, R. L., and Torres, O.: Incorporating the effect of small-scale circulations upon dust emission in an atmospheric general circulation model, Journal of Geophysical Research: Atmospheres, 109, https://doi.org/10.1029/2003jd004067, 2004.

Cheng, T., Peng, Y., Feichter, J., and Tegen, I.: An improvement on the dust emission scheme in the global aerosol-climate model ECHAM5-HAM, Atmospheric Chemistry and Physics, 8, 1105–1117, https://doi.org/10.5194/acp-8-1105-2008, 2008.

Cowie, S. M., Marsham, J. H., and Knippertz, P.: The importance of rare, high-wind events for dust uplift in northern Africa, Geophysical Research Letters, 42, 8208–8215, https://doi.org/10.1002/2015GL065819, 2015.

Csavina, J., Field, J., Félix, O., Corral-Avitia, A. Y., Sáez, A. E., and Betterton, E. A.: Effect of wind speed and relative humidity on atmospheric dust concentrations in semi-arid climates, Science of the Total Environment, 487, 82–90, https://doi.org/10.1016/j.scitotenv.2014.03.138, 2014.

Engelstaedter, S., Kohfeld, K. E., Tegen, I., and Harrison, S. P.: Controls of dust emissions by vegetation and topographic depressions: An evaluation using dust storm frequency data, Geophysical Research Letters, 30, https://doi.org/10.1029/2002GL016471, 2003.

Evan, A. T.: Surface Winds and Dust Biases in Climate Models, Geophysical Research Letters, 45, 1079–1085, https://doi.org/10.1002/2017GL076353, 2018.

Evan, A. T., Flamant, C., Fiedler, S., and Doherty, O.: An analysis of aeolian dust in climate models, Geophysical Research Letters, 41, 5996–6001, https://doi.org/10.1002/2014GL060545, 2014.

Evans, S., Ginoux, P., Malyshev, S., and Shevliakova, E.: Climate-vegetation interaction and amplification of Australian dust variability, Geophysical Research Letters, 43, 823–11, https://doi.org/10.1002/2016GL071016, 2016.

Fécan, F., Marticorena, B., and Bergametti, G.: Parametrization of the increase of the aeolian erosion threshold wind friction velocity due to soil moisture for arid and semi-arid areas, Annales Geophysicae, 17, 149, https://doi.org/10.1007/s005850050744, 1999.

Feng, Y., Wang, H., Rasch, P. J., Zhang, K., Lin, W., Tang, Q., Xie, S., Hamilton, D. S., Mahowald, N., and Yu, H.: Global Dust Cycle and Direct Radiative Effect in E3SM Version 1: Impact of Increasing Model Resolution, Journal of Advances in Modeling Earth Systems, https://doi.org/10.1029/2021MS002909, 2022.

Gelaro, R., McCarty, W., Suárez, M. J., Todling, R., Molod, A., Takacs, L., Randles, C. A., Darmenov, A., Bosilovich, M. G., Reichle, R., Wargan, K., Coy, L., Cullather, R., Draper, C., Akella, S., Buchard, V., Conaty, A., da Silva, A. M., Gu, W., Kim, G. K., Koster, R., Lucchesi, R., Merkova, D., Nielsen, J. E., Partyka, G., Pawson, S., Putman, W., Rienecker, M., Schubert, S. D., Sienkiewicz, M., and Zhao, B.: The modern-era retrospective analysis for research and applications, version 2 (MERRA-2), Journal of Climate, 30, 5419–5454, https://doi.org/10.1175/JCLI-D-16-0758.1, 2017.

Gettelman, A., Mills, M. J., Kinnison, D. E., Garcia, R. R., Smith, A. K., Marsh, D. R., Tilmes, S., Vitt, F., Bardeen, C. G., McInerny, J., Liu, H. L., Solomon, S. C., Polvani, L. M., Emmons, L. K., Lamarque, J. F., Richter, J. H., Glanville, A. S., Bacmeister, J. T., Phillips, A. S., Neale, R. B., Simpson, I. R., DuVivier, A. K., Hodzic, A., and Randel, W. J.: The Whole Atmosphere Community Climate Model Version 6 (WACCM6), Journal of Geophysical Research: Atmospheres, 124, 12 380–12 403, https://doi.org/10.1029/2019JD030943, 2019.

Ginoux, P., Chin, M., Tegen, I., Prospero, J. M., Holben, B., Dubovik, O., and Lin, S. J.: Sources and distributions of dust aerosols simulated with the GOCART model, Journal of Geophysical Research Atmospheres, 106, 20 255–20 273, https://doi.org/10.1029/2000JD000053, 2001.

Ginoux, P., Prospero, J. M., Gill, T. E., Hsu, N. C., and Zhao, M.: Global-scale attribution of anthropogenic and natural dust sources and their emission rates based on MODIS Deep Blue aerosol products, Reviews of Geophysics, 50, https://doi.org/10.1029/2012RG000388, 2012.

Gliß, J., Mortier, A., Schulz, M., Andrews, E., Balkanski, Y., Bauer, S. E., Benedictow, A. M., Bian, H., Checa-Garcia, R., Chin, M., Ginoux, P., Griesfeller, J. J., Heckel, A., Kipling, Z., Kirkeväg, A., Kokkola, H., Laj, P., Le Sager, P., Tronstad Lund, M., Lund Myhre, C., Matsui, H., Myhre, G., Neubauer, D., Van Noije, T., North, P., Olivié, D. J., Rémy, S., Sogacheva, L., Takemura, T., Tsigaridis, K., and Tsyro, S. G.: AeroCom phase III multi-model evaluation of the aerosol life cycle and optical properties using ground- And space-based remote sensing as well as surface in situ observations, Atmospheric Chemistry and Physics, 21, 87–128, https://doi.org/10.5194/acp-21-87-2021, 2021.

Grini, A., Myhre, G., Zender, C. S., and Isaksen, I. S.: Model simulations of dust sources and transport in the global atmosphere: Effects of soil erodibility and wind speed variability, Journal of Geophysical Research D: Atmospheres, 110, 1–14, https://doi.org/10.1029/2004JD005037, 2005.

Hajima, T., Watanabe, M., Yamamoto, A., Tatebe, H., Noguchi, M. A., Abe, M., Ohgaito, R., Ito, A., Yamazaki, D., Okajima, H., Ito, A., Takata, K., Ogochi, K., Watanabe, S., and Kawamiya, M.: Development of the MIROC-ES2L Earth system model and the evaluation of biogeochemical processes and feedbacks, Geoscientific Model Development, 13, 2197–2244, https://doi.org/10.5194/gmd-13-2197-2020, 2020.

Huneeus, N., Schulz, M., Balkanski, Y., Griesfeller, J., Prospero, J., Kinne, S., Bauer, S., Boucher, O., Chin, M., Dentener, F., Diehl, T., Easter, R., Fillmore, D., Ghan, S., Ginoux, P., Grini, A., Horowitz, L., Koch, D., Krol, M. C., Landing, W., Liu, X., Mahowald, N., Miller, R., Morcrette, J. J., Myhre, G., Penner, J., Perlwitz, J., Stier, P., Takemura, T., and Zender, C. S.: Global dust model intercomparison in AeroCom phase i, Atmospheric Chemistry and Physics, 11, 7781–7816, https://doi.org/10.5194/acp-11-7781-2011, 2011.

Kim, D., Chin, M., Yu, H., Diehl, T., Tan, Q., Kahn, R. A., Tsigaridis, K., Bauer, S. E., Takemura, T., Pozzoli, L., Bellouin, N., Schulz, M., Peyridieu, S., Chédin, A., and Koffi, B.: Sources, sinks, and transatlantic transport of North African dust aerosol: A multimodel analysis and comparison with remote sensing data, Journal of Geophysical Research, 119, 6259–6277, https://doi.org/10.1002/2013JD021099, 2014.

Kim, D., Chin, M., Schuster, G., Yu, H., Takemura, T., Tuccella, P., Ginoux, P., Liu, X., Shi, Y., Matsui, H., Tsigaridis, K., Bauer, S. E., Kok, J. F., and Schulz, M.: Where Dust Comes From: Global Assessment of Dust Source Attributions With AeroCom Models, Journal of Geophysical Research: Atmospheres, 129, e2024JD041 377, https://doi.org/https://doi.org/10.1029/2024JD041377, 2024.

Kim, H. and Choi, M.: Impact of soil moisture on dust outbreaks in East Asia: Using satellite and assimilation data, Geophysical Research Letters, 42, 2789–2796, https://doi.org/https://doi.org/10.1002/2015GL063325, 2015.

Knippertz, P.: Meteorological aspects of dust storms, in: Mineral Dust: A Key Player in the Earth System, pp. 121–147, Springer Dordrecht, ISBN 9789401789783, https://doi.org/10.1007/978-94-017-8978-3_6, 2014.

Knippertz, P. and Todd, M. C.: Mineral dust aerosols over the Sahara: Meteorological controls on emission and transport and implications for modeling, Reviews of Geophysics, 50, https://doi.org/10.1029/2011RG000362, 2012.

Kok, J. F., Albani, S., Mahowald, N. M., and Ward, D. S.: An improved dust emission model - Part 2: Evaluation in the Community Earth System Model, with implications for the use of dust source functions, Atmospheric Chemistry and Physics, 14, 13 043–13 061, https://doi.org/10.5194/acp-14-13043-2014, 2014a.

Kok, J. F., Mahowald, N. M., Fratini, G., Gillies, J. A., Ishizuka, M., Leys, J. F., Mikami, M., Park, M. S., Park, S. U., Van Pelt, R. S., and Zobeck, T. M.: An improved dust emission model - Part 1: Model description and comparison against measurements, Atmospheric Chemistry and Physics, 14, 13 023–13 041, https://doi.org/10.5194/acp-14-13023-2014, 2014b.

Kok, J. F., Storelvmo, T., Karydis, V. A., Adebiyi, A. A., Mahowald, N. M., Evan, A. T., He, C., and Leung, D. M.: Mineral dust aerosol impacts on global climate and climate change, Nature Reviews Earth and Environment, 4, 71–86, https://doi.org/10.1038/s43017-022-00379-5, 2023.

Koster, R. D., Guo, Z., Yang, R., Dirmeyer, P. A., Mitchell, K., and Puma, M. J.: On the nature of soil moisture in land surface models, Journal of Climate, 22, 4322–4335, https://doi.org/10.1175/2009JCLI2832.1, 2009.

Lee, E.-H. and Sohn, B.-J.: Examining the impact of wind and surface vegetation on the Asian dust occurrence over three classified source regions, Journal of Geophysical Research, 114, https://doi.org/10.1029/2008jd010687, 2009.

Leung, D. M., Kok, J. F., Li, L., Lawrence, D. M., Mahowald, N. M., Tilmes, S., and Kluzek, E.: A global dust emission dataset for estimating dust radiative forcings in climate models, Atmos. Chem. Phys., 25, 2311–2331, https://doi.org/10.5194/acp-25-2311-2025, 2025.

Li, L., Mahowald, N. M., Kok, J. F., Liu, X., Wu, M., Leung, D. M., Hamilton, D. S., Emmons, L. K., Huang, Y., Sexton, N., Meng, J., and Wan, J.: Importance of different parameterization changes for the updated dust cycle modeling in the Community Atmosphere Model (version 6.1), Geoscientific Model Development, 15, 8181–8219, https://doi.org/10.5194/gmd-15-8181-2022, 2022a.

Li, L., Mahowald, N. M., Gonçalves Ageitos, M., Obiso, V., Miller, R. L., Pérez García-Pando, C., Di Biagio, C., Formenti, P., Brodrick, P. G., Clark, R. N., Green, R. O., Kokaly, R., Swayze, G., and Thompson, D. R.: Improved constraints on hematite refractive index for

estimating climatic effects of dust aerosols, Communications Earth & Environment, 5, 295, https://doi.org/10.1038/s43247-024-01441-4, 2024.

Li, X., Zhang, Y. J., Gao, H., and Ding, T.: Extreme cold wave in early November 2021 in China and the influences from the meridional pressure gradient over East Asia, Advances in Climate Change Research, 13, 797–802, https://doi.org/10.1016/j.accre.2022.11.011, 2022b.

Lu, H. and Shao, Y.: A new model for dust emission by saltation bombardment, Journal of Geophysical Research Atmospheres, 104, 16 827–16 842, https://doi.org/10.1029/1999JD900169, 1999.

Lurton, T., Balkanski, Y., Bastrikov, V., Bekki, S., Bopp, L., Braconnot, P., Brockmann, P., Cadule, P., Contoux, C., Cozic, A., Cugnet, D., Dufresne, J.-L., Éthé, C., Foujols, M.-A., Ghattas, J., Hauglustaine, D., Hu, R.-M., Kageyama, M., Khodri, M., Lebas, N., Levavasseur, G., Marchand, M., Ottlé, C., Peylin, P., Sima, A., Szopa, S., Thiéblemont, R., Vuichard, N., and Boucher, O.: Implementation of the CMIP6 Forcing Data in the IPSL-CM6A-LR Model, Journal of Advances in Modeling Earth Systems, 12, e2019MS001 940, https://doi.org/https://doi.org/10.1029/2019MS001940, 2020.

Marticorena, B. and Bergametti, G.: Modeling the atmospheric dust cycle: 1. Design of a soil-derived dust emission scheme, Journal of Geophysical Research, 100, https://doi.org/10.1029/95jd00690, 1995.

Mauritsen, T., Bader, J., Becker, T., Behrens, J., Bittner, M., Brokopf, R., Brovkin, V., Claussen, M., Crueger, T., Esch, M., Fast, I., Fiedler, S., Fläschner, D., Gayler, V., Giorgetta, M., Goll, D. S., Haak, H., Hagemann, S., Hedemann, C., Hohenegger, C., Ilyina, T., Jahns, T., Jimenéz-de-la Cuesta, D., Jungclaus, J., Kleinen, T., Kloster, S., Kracher, D., Kinne, S., Kleberg, D., Lasslop, G., Kornblueh, L., Marotzke, J., Matei, D., Meraner, K., Mikolajewicz, U., Modali, K., Möbis, B., Müller, W. A., Nabel, J. E. M. S., Nam, C. C. W., Notz, D., Nyawira, S.-S., Paulsen, H., Peters, K., Pincus, R., Pohlmann, H., Pongratz, J., Popp, M., Raddatz, T. J., Rast, S., Redler, R., Reick, C. H., Rohrschneider, T., Schemann, V., Schmidt, H., Schnur, R., Schulzweida, U., Six, K. D., Stein, L., Stemmler, I., Stevens, B., von Storch, J.-S., Tian, F., Voigt, A., Vrese, P., Wieners, K.-H., Wilkenskjeld, S., Winkler, A., and Roeckner, E.: Developments in the MPI-M Earth System Model version 1.2 (MPI-ESM1.2) and Its Response to Increasing CO2, Journal of Advances in Modeling Earth Systems, 11, 998–1038, https://doi.org/https://doi.org/10.1029/2018MS001400, 2019.

Miller, R. L., Cakmur, R. V., Perlwitz, J., Geogdzhayev, I. V., Ginoux, P., Koch, D., Kohfeld, K. E., Prigent, C., Ruedy, R., Schmidt, G. A., and Tegen, I.: Mineral dust aerosols in the NASA Goddard Institute for Space Sciences ModelE atmospheric general circulation model, Journal of Geophysical Research Atmospheres, 111, https://doi.org/10.1029/2005JD005796, 2006.

Miller, R. L., Schmidt, G. A., Nazarenko, L. S., Bauer, S. E., Kelley, M., Ruedy, R., Russell, G. L., Ackerman, A. S., Aleinov, I., Bauer, M., Bleck, R., Canuto, V., Cesana, G., Cheng, Y., Clune, T. L., Cook, B. I., Cruz, C. A., Del Genio, A. D., Elsaesser, G. S., Faluvegi, G., Kiang, N. Y., Kim, D., Lacis, A. A., Leboissetier, A., LeGrande, A. N., Lo, K. K., Marshall, J., Matthews, E. E., McDermid, S., Mezuman, K., Murray, L. T., Oinas, V., Orbe, C., Pérez García-Pando, C., Perlwitz, J. P., Puma, M. J., Rind, D., Romanou, A., Shindell, D. T., Sun, S., Tausnev, N., Tsigaridis, K., Tselioudis, G., Weng, E., Wu, J., and Yao, M. S.: CMIP6 Historical Simulations (1850–2014) With GISS-E2.1, Journal of Advances in Modeling Earth Systems, 13, https://doi.org/10.1029/2019MS002034, 2021.

Nabat, P., Somot, S., Mallet, M., Michou, M., Sevault, F., Driouech, F., Meloni, D., Di Sarra, A., Di Biagio, C., Formenti, P., Sicard, M., Léon, J. F., and Bouin, M. N.: Dust aerosol radiative effects during summer 2012 simulated with a coupled regional aerosol-atmosphere-ocean model over the Mediterranean, Atmospheric Chemistry and Physics, 15, 3303–3326, https://doi.org/10.5194/acp-15-3303-2015, 2015.

Nandintsetseg, B. and Shinoda, M.: Land surface memory effects on dust emission in a Mongolian temperate grassland, Journal of Geophysical Research: Biogeosciences, 120, 414–427, https://doi.org/10.1002/2014JG002708, 2015.

Peng, Y., Von Salzen, K., and Li, J.: Simulation of mineral dust aerosol with Piecewise Log-normal Approximation (PLA) in CanAM4-PAM, Atmospheric Chemistry and Physics, 12, 6891–6914, https://doi.org/10.5194/acp-12-6891-2012, 2012.

Prospero, J. M. and Lamb, P. J.: African Droughts and Dust Transport to the Caribbean: Climate Change Implications, Science, 302, 1024–1027, https://doi.org/10.1126/science.1089915, 2003.

Prospero, J. M., Ginoux, P., Torres, O., Nicholson, S. E., and Gill, T. E.: Environmental characterization of global sources of atmospheric soil dust identified with the Nimbus 7 Total Ozone Mapping Spectrometer (TOMS) absorbing aerosol product, Reviews of Geophysics, 40, 2–1, https://doi.org/10.1029/2000RG000095, 2002.

Pu, B. and Ginoux, P.: The impact of the Pacific Decadal Oscillation on springtime dust activity in Syria, Atmospheric Chemistry and Physics, 16, 13 431–13 448, https://doi.org/10.5194/acp-16-13431-2016, 2016.

Pu, B. and Ginoux, P.: How reliable are CMIP5 models in simulating dust optical depth?, Atmospheric Chemistry and Physics, 18, 12 491–12 510, https://doi.org/10.5194/acp-18-12491-2018, 2018.

Randles, C. A., da Silva, A. M., Buchard, V., Colarco, P. R., Darmenov, A., Govindaraju, R., Smirnov, A., Holben, B., Ferrare, R., Hair, J., Shinozuka, Y., and Flynn, C. J.: The MERRA-2 aerosol reanalysis, 1980 onward. Part I: System description and data assimilation evaluation, Journal of Climate, 30, 6823–6850, https://doi.org/10.1175/JCLI-D-16-0609.1, 2017.

Ravi, S., D'Odorico, P., Over, T. M., and Zobeck, T. M.: On the effect of air humidity on soil susceptibility to wind erosion: The case of air-dry soils, Geophysical Research Letters, 31, https://doi.org/10.1029/2004GL019485, 2004.

RAVI, S., ZOBECK, T. E. D. M., OVER, T. M., OKIN, G. S., and D'ODORICO, P.: On the effect of moisture bonding forces in air-dry soils on threshold friction velocity of wind erosion, Sedimentology, 53, 597–609, https://doi.org/https://doi.org/10.1111/j.1365-3091.2006.00775.x, 2006.

Ridley, D. A., Heald, C. L., Pierce, J. R., and Evans, M. J.: Toward resolution-independent dust emissions in global models: Impacts on the seasonal and spatial distribution of dust, Geophysical Research Letters, 40, 2873–2877, https://doi.org/10.1002/grl.50409, 2013.

Rind, D., Orbe, C., Jonas, J., Nazarenko, L., Zhou, T., Kelley, M., Lacis, A., Shindell, D., Faluvegi, G., Romanou, A., Russell, G., Tausnev, N., Bauer, M., and Schmidt, G.: GISS Model E2.2: A Climate Model Optimized for the Middle Atmosphere—Model Structure, Climatology, Variability, and Climate Sensitivity, Journal of Geophysical Research: Atmospheres, 125, https://doi.org/10.1029/2019JD032204, 2020.

Roberts, M. J., Baker, A., Blockley, E. W., Calvert, D., Coward, A., Hewitt, H. T., Jackson, L. C., Kuhlbrodt, T., Mathiot, P., Roberts, C. D., Schiemann, R., Seddon, J., Vannière, B., and Vidale, P. L.: Description of the resolution hierarchy of the global coupled HadGEM3-GC3.1 model as used in CMIP6 HighResMIP experiments, Geosci. Model Dev., 12, 4999–5028, https://doi.org/10.5194/gmd-12-4999-2019, 2019.

Schulz, M., Cozic, A., and Szopa, S.: LMDzT-INCA dust forecast model developments and associated validation efforts, IOP Conference Series: Earth and Environmental Science, 7, 012 014, https://doi.org/10.1088/1755-1307/7/1/012014, 2009.

Séférian, R., Nabat, P., Michou, M., Saint-Martin, D., Voldoire, A., Colin, J., Decharme, B., Delire, C., Berthet, S., Chevallier, M., Sénési, S., Franchisteguy, L., Vial, J., Mallet, M., Joetzjer, E., Geoffroy, O., Guérémy, J. F., Moine, M. P., Msadek, R., Ribes, A., Rocher, M., Roehrig, R., Salas-y Mélia, D., Sanchez, E., Terray, L., Valcke, S., Waldman, R., Aumont, O., Bopp, L., Deshayes, J., Éthé, C., and Madec, G.: Evaluation of CNRM Earth System Model, CNRM-ESM2-1: Role of Earth System Processes in Present-Day and Future Climate, Journal of Advances in Modeling Earth Systems, 11, 4182–4227, https://doi.org/10.1029/2019MS001791, 2019.

Seland, O., Bentsen, M., Olivié, D., Toniazzo, T., Gjermundsen, A., Graff, L. S., Debernard, J. B., Gupta, A. K., He, Y. C., Kirkeväg, A., Schwinger, J., Tjiputra, J., Schanke Aas, K., Bethke, I., Fan, Y., Griesfeller, J., Grini, A., Guo, C., Ilicak, M., Karset, I. H. H., Landgren, O., Liakka, J., Moseid, K. O., Nummelin, A., Spensberger, C., Tang, H., Zhang, Z., Heinze, C., Iversen, T., and Schulz, M.: Overview of the Norwegian Earth System Model (NorESM2) and key climate response of CMIP6 DECK, historical, and scenario simulations, Geoscientific Model Development, 13, 6165–6200, https://doi.org/10.5194/gmd-13-6165-2020, 2020.

Shao, Y. and Lu, H.: A simple expression for wind erosion threshold friction velocity, Journal of Geophysical Research Atmospheres, 105, 22 437–22 443, https://doi.org/10.1029/2000JD900304, 2000.

Shao, Y., Raupach, M. R., and Leys, J. F.: A model for predicting aeolian sand drift and dust entrainment on scales from paddock to region, Australian Journal of Soil Research, 34, 309–342, https://doi.org/10.1071/SR9960309, 1996.

Shao, Y., Wyrwoll, K. H., Chappell, A., Huang, J., Lin, Z., McTainsh, G. H., Mikami, M., Tanaka, T. Y., Wang, X., and Yoon, S.: Dust cycle: An emerging core theme in Earth system science, Aeolian Research, 2, 181–204, https://doi.org/10.1016/j.aeolia.2011.02.001, 2011.

Shevliakova, E., Malyshev, S., Martinez-Cano, I., Milly, P. C. D., Pacala, S. W., Ginoux, P., Dunne, K. A., Dunne, J. P., Dupuis, C., Findell, K. L., Ghannam, K., Horowitz, L. W., Knutson, T. R., Krasting, J. P., Naik, V., Phillipps, P., Zadeh, N., Yu, Y., Zeng, F., and Zeng, Y.: The Land Component LM4.1 of the GFDL Earth System Model ESM4.1: Model Description and Characteristics of Land Surface Climate and Carbon Cycling in the Historical Simulation, Journal of Advances in Modeling Earth Systems, 16, e2023MS003 922, https://doi.org/https://doi.org/10.1029/2023MS003922, 2024.

Shinoda, M., Gillies, J. A., Mikami, M., and Shao, Y.: Temperate grasslands as a dust source: Knowledge, uncertainties, and challenges, Aeolian Research, 3, 271–293, https://doi.org/10.1016/j.aeolia.2011.07.001, 2011.

Sigmond, M., Anstey, J., Arora, V., Digby, R., Gillett, N., Kharin, V., Merryfield, W., Reader, C., Scinocca, J., Swart, N., Virgin, J., Abraham, C., Cole, J., Lambert, N., Lee, W. S., Liang, Y., Malinina, E., Rieger, L., Von Salzen, K., Seiler, C., Seinen, C., Shao, A., Sospedra-Alfonso, R., Wang, L., and Yang, D.: Improvements in the Canadian Earth System Model (CanESM) through systematic model analysis: CanESM5.0 and CanESM5.1, Geoscientific Model Development, 16, 6553–6591, https://doi.org/10.5194/gmd-16-6553-2023, 2023.

Sokolik, I. N., Darmenova, K., Huang, J., Kalashnikova, O., Kurosaki, Y., and Xi, X.: Examining changes in land cover and land use, regional climate and dust in Dryland East Asia and Their Linkages within the Earth System, in: Dryland East Asia: Land Dynamics amid Social and Climate Change, edited by Chen, J., Wan, S., Henebry, G., Qi, J., Gutman, G., Sun, G., and Kappas, M., chap. 9, pp. 183–211, DE GRUYTER, Berlin, Boston, ISBN 9783110287912, https://doi.org/10.1515/9783110287912.183, 2021.

Szopa, S., Balkanski, Y., Schulz, M., Bekki, S., Cugnet, D., Fortems-Cheiney, A., Turquety, S., Cozic, A., Déandreis, C., Hauglustaine, D., Idelkadi, A., Lathière, J., Lefevre, F., Marchand, M., Vuolo, R., Yan, N., and Dufresne, J. L.: Aerosol and ozone changes as forcing for climate evolution between 1850 and 2100, Climate Dynamics, 40, 2223–2250, https://doi.org/10.1007/s00382-012-1408-y, 2013.

Takemura, T., Egashira, M., Matsuzawa, K., Ichijo, H., O'Ishi, R., and Abe-Ouchi, A.: A simulation of the global distribution and radiative forcing of soil dust aerosols at the Last Glacial Maximum, Atmospheric Chemistry and Physics, 9, 3061–3073, https://doi.org/10.5194/acp-9-3061-2009, 2009.

Tatebe, H., Ogura, T., Nitta, T., Komuro, Y., Ogochi, K., Takemura, T., Sudo, K., Sekiguchi, M., Abe, M., Saito, F., Chikira, M., Watanabe, S., Mori, M., Hirota, N., Kawatani, Y., Mochizuki, T., Yoshimura, K., Takata, K., O'Ishi, R., Yamazaki, D., Suzuki, T., Kurogi, M., Kataoka, T., Watanabe, M., and Kimoto, M.: Description and basic evaluation of simulated mean state, internal variability, and climate sensitivity in MIROC6, Geoscientific Model Development, 12, 2727–2765, https://doi.org/10.5194/gmd-12-2727-2019, 2019.

Tegen, I., Harrison, S. P., Kohfeld, K., Prentice, I. C., Coe, M., and Heimann, M.: Impact of vegetation and preferential source areas on global dust aerosol: Results from a model study, Journal of Geophysical Research Atmospheres, 107, https://doi.org/10.1029/2001JD000963, 2002.

Tegen, I., Neubauer, D., Ferrachat, S., Drian, C. S. L., Bey, I., Schutgens, N., Stier, P., Watson-Parris, D., Stanelle, T., Schmidt, H., Rast, S., Kokkola, H., Schultz, M., Schroeder, S., Daskalakis, N., Barthel, S., Heinold, B., and Lohmann, U.: The global aerosol-climate model echam6.3-ham2.3 -Part 1: Aerosol evaluation, Geoscientific Model Development, 12, 1643–1677, https://doi.org/10.5194/gmd-12-1643-2019, 2019.

Textor, C., Schulz, M., Guibert, S., Kinne, S., Balkanski, Y., Bauer, S., Berntsen, T., Berglen, T., Boucher, O., Chin, M., Dentener, F., Diehl, T., Easter, R., Feichter, H., Fillmore, D., Ghan, S., Ginoux, P., Gong, S., Grini, A., Hendricks, J., Horowitz, L., Huang, P., Isaksen, I., Iversen, T., Kloster, S., Koch, D., Kirkevåg, A., Kristjansson, J. E., Krol, M., Lauer, A., Lamarque, J. F., Liu, X., Montanaro, V., Myhre, G., Penner, J., Pitari, G., Reddy, S., Seland, Stier, P., Takemura, T., and Tie, X.: Analysis and quantification of the diversities of aerosol life cycles within AeroCom, Atmospheric Chemistry and Physics, 6, 1777–1813, https://doi.org/10.5194/acp-6-1777-2006, 2006.

Van Noije, T., Bergman, T., Le Sager, P., O'Donnell, D., Makkonen, R., Gonçalves-Ageitos, M., Döscher, R., Fladrich, U., Von Hardenberg, J., Keskinen, J. P., Korhonen, H., Laakso, A., Myriokefalitakis, S., Ollinaho, P., Pérez Garciá-Pando, C., Reerink, T., Schrödner, R., Wyser, K., and Yang, S.: EC-Earth3-AerChem: A global climate model with interactive aerosols and atmospheric chemistry participating in CMIP6, Geoscientific Model Development, 14, 5637–5668, https://doi.org/10.5194/gmd-14-5637-2021, 2021.

Volodin, E. M.: Possible Climate Change in Russia in the 21st Century Based on the INM-CM5-0 Climate Model, Russian Meteorology and Hydrology, 47, 327–333, https://doi.org/10.3103/S1068373922050016, 2022.

Volodin, E. M. and Kostrykin, S. V.: The aerosol module in the INM RAS climate model, Russian Meteorology and Hydrology, 41, 519–528, https://doi.org/10.3103/S106837391608001X, 2016.

Woodward, S.: Modeling the atmospheric life cycle and radiative impact of mineral dust in the Hadley Centre climate model, Journal of Geophysical Research Atmospheres, 106, 18 155–18 166, https://doi.org/10.1029/2000JD900795, 2001.

Woodward, S.: Hadley Centre Technical Note 87 - Mineral dust in HadGEM2, Tech. rep., Met Office, Exeter, 2011.

Woodward, S., Sellar, A. A., Tang, Y., Stringer, M., Yool, A., Robertson, E., and Wiltshire, A.: The simulation of mineral dust in the United Kingdom Earth System Model UKESM1, Atmospheric Chemistry and Physics, 22, 14 503–14 528, https://doi.org/10.5194/acp-22-14503-2022, 2022.

Wu, C., Lin, Z., Liu, X., Li, Y., Lu, Z., and Wu, M.: Can Climate Models Reproduce the Decadal Change of Dust Aerosol in East Asia?, Geophysical Research Letters, 45, 9953–9962, https://doi.org/10.1029/2018GL079376, 2018.

Wu, C., Lin, Z., and Liu, X.: The global dust cycle and uncertainty in CMIP5 (Coupled Model Intercomparison Project phase 5) models, Atmospheric Chemistry and Physics, 20, 10 401–10 425, https://doi.org/10.5194/acp-20-10401-2020, 2020.

Xi, X.: On the Geomorphic, Meteorological, and Hydroclimatic Drivers of the Unusual 2018 Early Summer Salt Dust Storms in Central Asia, Journal of Geophysical Research: Atmospheres, 128, https://doi.org/10.1029/2022JD038089, 2023.

Xi, X. and Sokolik, I. N.: Seasonal dynamics of threshold friction velocity and dust emission in Central Asia, Journal of Geophysical Research: Atmospheres, 120, 1536–1564, https://doi.org/10.1002/2014JD022471, 2015a.

Xi, X. and Sokolik, I. N.: Dust interannual variability and trend in Central Asia from 2000 to 2014 and their climatic linkages, Journal of Geophysical Research: Atmospheres, 120, 12 175–12 197, https://doi.org/10.1002/2015JD024092, 2015b.

Xie, S., Terai, C., Wang, H., Tang, Q., Fan, J., Burrows, S., Lin, W., Wu, M., Song, X., Zhang, Y., Taylor, M., Golaz, J.-C., Benedict, J., Chen, C.-C., Feng, Y., Hannah, W., Ke, Z., Shan, Y., Larson, V., and Bader, D.: The Energy Exascale Earth System Model Version 3. Part I: Overview of the Atmospheric Component, Under Review, https://doi.org/10.22541/essoar.174456922.21825772/v1, 2025.

Yukimoto, S., Kawai, H., Koshiro, T., Oshima, N., Yoshida, K., Urakawa, S., Tsujino, H., Deushi, M., Tanaka, T., Hosaka, M., Yabu, S., Yoshimura, H., Shindo, E., Mizuta, R., Obata, A., Adachi, Y., and Ishii, M.: The meteorological research institute Earth system model version 2.0, MRI-ESM2.0: Description and basic evaluation of the physical component, Journal of the Meteorological Society of Japan, 97, 931–965, https://doi.org/10.2151/jmsj.2019-051, 2019.

Yumimoto, K., Tanaka, T. Y., Oshima, N., and Maki, T.: JRAero: The Japanese Reanalysis for Aerosol v1.0, Geoscientific Model Development, 10, 3225–3253, https://doi.org/10.5194/gmd-10-3225-2017, 2017.

Zender, C. S. and Kwon, E. Y.: Regional contrasts in dust emission responses to climate, Journal of Geophysical Research Atmospheres, 110, https://doi.org/10.1029/2004JD005501, 2005.

Zender, C. S., Bian, H., and Newman, D.: Mineral Dust Entrainment and Deposition (DEAD) model: Description and 1990s dust climatology, Journal of Geophysical Research: Atmospheres, 108, https://doi.org/10.1029/2002jd002775, 2003.

Zhang, J., Teng, Z., Huang, N., Guo, L., and Shao, Y.: Surface renewal as a significant mechanism for dust emission, Atmospheric Chemistry and Physics, 16, 15 517–15 528, https://doi.org/10.5194/acp-16-15517-2016, 2016a.

Zhang, K., Zhao, C., Wan, H., Qian, Y., Easter, R. C., Ghan, S. J., Sakaguchi, K., and Liu, X.: Quantifying the impact of sub-grid surface wind variability on sea salt and dust emissions in CAM5, Geoscientific Model Development, 9, 607–632, https://doi.org/10.5194/gmd-9-607-2016, 2016b.

Zhao, A., Ryder, C. L., and Wilcox, L. J.: How well do the CMIP6 models simulate dust aerosols?, Atmospheric Chemistry and Physics, 22, 2095–2119, https://doi.org/10.5194/acp-22-2095-2022, 2022.

Zomer, R. J., Xu, J., and Trabucco, A.: Version 3 of the Global Aridity Index and Potential Evapotranspiration Database, Scientific Data, 9, https://doi.org/10.1038/s41597-022-01493-1, 2022.

Zou, X. K. and Zhai, P. M.: Relationship between vegetation coverage and spring dust storms over northern China, Journal of Geophysical Research: Atmospheres, 109, https://doi.org/10.1029/2003jd003913, 2004.